Exact Performance Analysis of Ambient RF Energy Harvesting Wireless Sensor Networks With Ginibre Point Process

Han-Bae Kong, *Member, IEEE*, Ian Flint, Ping Wang, *Senior Member, IEEE*, Dusit Niyato, *Senior Member, IEEE*, and Nicolas Privault

***Abstract*—Ambient radio frequency (RF) energy harvesting methods have drawn significant interests due to their ability to provide energy to wireless devices from ambient RF sources. This paper considers ambient RF energy harvesting wireless sensor networks where a sensor node transmits data to a data sink using the energy harvested from the signals transmitted by the ambient RF sources. We analyze the performance of the network, i.e., the mean of the harvested energy, the power outage probability and the transmission outage probability. In many practical networks, the locations of the ambient RF sources are spatially correlated and the ambient sources exhibit repulsive behaviors. Therefore, we model the spatial distribution of the ambient sources as an α-Ginibre point process (α-GPP) which reflects the repulsion among the RF sources and includes the Poisson point process as a special case. We also assume that the fading channel is Nakagami-m distributed, which also includes Rayleigh fading as a particular case. In this paper, by exploiting the Laplace transform of the α-GPP, we introduce semi-closed-form expressions for the considered performance metrics and provide an upper bound of the power outage probability. The derived expressions are expressed in terms of the Fredholm determinant which can be computed numerically. In order to reduce the complexity in computing the Fredholm determinant, we provide a simple closed-form expression for the Fredholm determinant which allows us to evaluate the Fredholm determinant much more efficiently. The accuracy of our analytical results is validated through simulation results.**

***Index Terms*—Energy harvesting, green communications, repulsive point process, Ginibre point process, stochastic geometry.**

I. Introduction

Recently, there has been a lot of research interest on the topic of radio frequency (RF) energy harvesting techniques which convert energy of RF signals into direct current (DC) power for device operation [1], [2]. Since it enables energy-constrained wireless devices to replenish energy from the RF signals and prolongs the life time of the devices, various RF energy harvesting wireless networks were investigated in [3]–[6]. There are mainly two types of RF energy sources considered in the RF energy harvesting networks, i.e., dedicated RF sources and ambient RF sources.

When dedicated RF sources are employed, energy harvesting devices scavenge power from the RF signals radiated by its dedicated RF energy transmitters. Lately, several transmission strategies which aim at optimizing the performance of networks with dedicated RF sources were developed in [7]–[11]. The authors in [7] studied a simultaneous wireless information and power transfer (SWIPT) technique which transmits both data and energy at the same time for a multiple-input multiple-output (MIMO) wireless broadcast system. A power splitting technique for an RF energy harvesting interference channel was proposed in [8]. Also, the works in [9] and [10] characterized tradeoff between the information rate and the harvested energy for two-user and K-user interference channels, respectively. Under the protocol of harvest-then-transmit, reference [11] provided the optimal beamforming and time allocation algorithm which maximizes the sum-throughput of multi-user systems.

Unlike the dedicated RF energy sources, ambient RF sources are nearby RF transmitters which do not intend to transmit RF power to energy harvesting devices. The ambient RF sources contain static sources such as cellular base stations, TV and radio towers, and dynamic sources such as WiFi routers and mobile devices [1]. Many experiments in [12]–[15] presented implementations of ambient RF energy harvesting techniques which charge wireless devices' batteries by harvesting the RF signals from WiFi, GSM, DTV bands and mobile devices. Based on these experimental results, several researchers examined the performance of ambient RF energy harvesting systems by leveraging stochastic geometry tools [16]–[24].

For uplink cellular systems where ambient energy sources are distributed according to a Poisson point process (PPP), the study in [16] investigated a tradeoff among transmit power, density of base stations, and density of energy sources, and the work in [17] analyzed the transmission success probability of the systems. The outage probability of relaying systems with a random relay selection policy was derived in [18] when both source and relay nodes are assumed to follow PPP distributions. In addition, the authors in [19] and [20] considered several relay selection schemes and examined the outage probability and diversity order of the relaying systems. In [21], the probability of successful data exchange and the network lifetime gain in two-way network coded

This work was supported in part by the Singapore MOE Tier 1 (MOE2015-T1-2-130 and RG18/13 12) and MOE Tier 2 (MOE2013-T2-2-070 ARC16/14 and MOE2014-T2-2-015 ARC 4/15).

H.-B. Kong, P. Wang and D. Niyato are with the School of Computer Science and Engineering, Nanyang Technological University, Singapore 639798 (e-mail: {hbkong, wangping, dniyato}@ntu.edu.sg).

I. Flint and N. Privault are with the School of Physical and Mathematical Sciences, Nanyang Technological University, Singapore 639798 (e-mail: {iflint, nprivault}@ntu.edu.sg). I. Flint is the corresponding author.

relaying networks were studied. Moreover, the performance of ambient RF energy harvesting cognitive radio networks was characterized in [22] and [23], and the outage probability of ad hoc networks where the locations of power beacons and information transmitters are modeled as independent PPPs was analyzed in [24].

Most previous works on ambient RF energy harvesting networks have assumed that the ambient RF sources follow a PPP due to its analytical tractability. However, in practical networks, as shown in [25]–[27], the ambient RF sources, such as mobile sensor networks, cellular base stations, exhibit repulsion behaviors, and thus there exists a form of correlation among the RF sources. Therefore, modeling the spatial distribution of RF sources as a PPP may not be sufficient for characterizing the performance of the practical networks. Although, point processes like the Matérn hard-core process [28] or Gibbs point process [29] can reflect this repulsion, these processes do not yield analytical expressions for the performance of the networks as their correlation functions and the corresponding Laplace transforms are unknown. To this end, recently, several researchers investigated wireless networks with determinantal point processes (DPPs) which can capture the repulsiveness and have attractive mathematical properties [30]–[34].

In this paper, we model the spatial distribution of ambient RF sources as a Ginibre point process (GPP) which is one of the most practical examples of two-dimensional DPPs [35], [36]. The authors in [31]–[33] studied cellular networks where base stations are deployed according to a β-GPP. Also, the worst-case performance of ambient RF harvesting networks was analyzed in [34] when the distribution of the ambient RF sources follows an α-GPP. The β-GPP $(0 < \beta \leq 1)$ is a thinned and re-scaled GPP which is obtained by deleting each point of the GPP independently and with probability $1-\beta$, and then applying the homothety of ratio $\sqrt{\beta}$ to the remaining points in order to maintain the original intensity of the GPP [31]. The β-GPP becomes the GPP when $\beta = 1$ and converges weakly to the PPP as $\beta \to 0$. On the other hand, the α-GPP $(-1 \leq \alpha < 0)$ is a superposition of $-1/\alpha$ independent copies of a GPP with an intensity rescaled by a factor of $\sqrt{-\alpha}$. The α-GPP corresponds to the GPP when α is set to $\alpha = -1$ and converges weakly to the PPP when $\alpha \to 0$. Therefore, both the α-GPP and the β-GPP generalize the GPP and contain the PPP as a special case. In this paper, we focus on the α-GPP since its construction by superposition of independent repulsive point processes is more suitable, as we interpret the repulsion as happening on distinct independent layers. Also, we note that our computations on the α-GPP are represented in terms of the Fredholm determinant [36], and identical results may be applied to the β-GPP setting with no major technical difficulties.

Lately, ambient RF energy harvesting sensor networks where a sensor node sends data to a data sink using the energy harvested from the signals radiated by the α-GPP distributed ambient RF sources were studied in [34]. The authors in [34] analyzed the worst-case performance of the networks under the assumptions that channels among nodes experience a free-space path loss, i.e., small-scale fading channels are constant, and the received signals at the sensor node and the data sink are the same. However, in practical networks, the power of received signal at a node is determined by not only the path loss but also channel fading characteristics. In addition, in [34] it is assumed that the sensor node and the data sink are very close to each other, since the distance from an RF source to the data sink is assumed to be equal to the distance from the RF source to the sensor node.

In this paper, we analyze the exact performance rather than the worst-case performance of ambient RF energy harvesting sensor networks where the spatial distribution of ambient RF sources follows an α-GPP, and under a Nakagami-m channel fading assumption. Our goal is to analyze the performance of energy harvesting networks by capturing the combined effects of randomness in both the locations of RF sources and the attenuation occurring on the channels.

We consider a harvest-then-transmit protocol where a battery-free sensor node transmits data to a data sink utilizing the instantaneously scavenged power. We first derive the Laplace transform of the harvested energy at the sensor node and analyze three performance metrics, i.e., the mean of the harvested energy, the power outage probability and the transmission outage probability. Our main contributions are summarized as follows:

- First, we derive a formula to compute the Laplace transforms of the harvested energy at the sensor node and the interference at the data sink where RF signals experience both path loss and channel fading. The derived Laplace transforms are given in terms of a Fredholm determinant, which is a concept that generalizes the conventional determinant of a matrix and can be numerically calculated. We also introduce a closed-form expression for the Fredholm determinant which enables us to evaluate the Fredholm determinant with a reduced complexity.
- Next, we provide a closed-form expression for the mean of the harvested energy at the sensor node which depends on the network parameters, i.e., the density of the RF sources, the transmit power at the RF sources, the RF-to-DC power conversion efficiency, and so on.
- Assuming that the channel between the different RF sources and the sensor node follows the Nakagami-m distribution, we derive semi-closed-form expressions for the power outage probability, i.e., the probability that the harvested energy at the sensor node is less than the minimum required power for base circuit operation. When the power outage happens, the sensor node becomes inactive, and thus a data transmission cannot occur. We additionally provide the probability density function (PDF) of the harvested energy and an upper bound of the power outage probability.
- Based on the derived PDF of the harvested energy, we investigate the transmission outage probability, i.e., the probability that the data transmission rate is less than a certain transmission rate requirement. In addition, we consider two transmission scenarios, i.e., in-band and out-of-band transmissions. We provide semi-closed-form expressions for the transmission outage probability for networks with Nakagami-m distributed channel fading

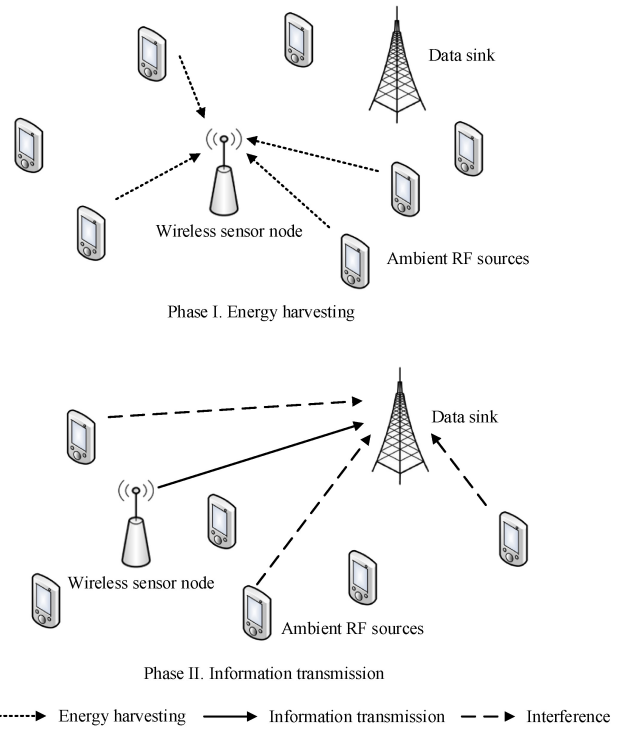

Fig. 1. Ambient RF energy haversting wireless sensor networks

and the constant channel fading.

It is confirmed that our analytical results are well matched with the Monte Carlo simulation results. By using the derived expressions, we are thus able to evaluate the performance of the networks in short simulation times.

The remainder of this paper is organized as follows. The system model is presented in Section II. In Section III, we introduce the fundamental properties of the DPP and the α-GPP, and provide a formula to compute the Laplace transform as well as a closed-form expression for the Fredholm determinant. Section IV analyzes the performance of the system and provides semi-closed-form expressions for the exact performance metrics and an upper bound of the power outage probability. In Section V, numerical results are illustrated to validate our analysis. Finally, the conclusions are drawn in Section VI.

Throughout the paper, we will use the following notations. The operators $\|\cdot\|$ and $\overline{x}$ are adopted to represent Euclidean 2-norm and the conjugate of a complex scalar x, respectively. In addition, $\mathbb{P}(A)$ and $\mathbb{E}[X]$ indicate the probability of an event A and the expectation of a random variable X, respectively.

II. System Model

In this paper, we consider ambient RF energy harvesting wireless sensor networks where a sensor node harvests power from the RF signals radiated by the ambient RF sources such as cellular mobiles, WiFi routers and TV towers, and transmits data to a data sink by using the harvested energy as shown in Fig. 1. The sensor node operates in a harvest-then-transmit protocol as described in Fig. 2, and in particular the sensor node scavenges energy for a time slot (Phase I) and sends

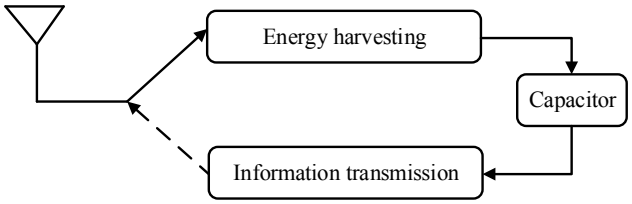

Fig. 2. Block diagram of harvest-then-transmit protocol

information to the data sink in the other time slot (Phase II). We assume that the locations of the ambient RF sources during a time slot are modeled as an α-GPP with a density λ and in an observation window $\mathcal{B}_{\mathbf{o}}(R)$ where $\mathcal{B}_{\mathbf{o}}(R)$ denotes a ball of radius R centered at $\mathbf{o} \in \mathbb{R}^2$, and the transmit power at the ambient nodes is P_A. We denote the spatial locations of the RF sources in the energy harvesting and information transmission phases by Φ and $\tilde{\Phi}$, respectively, and we assume that the RF signal transmitting sources in the two phases are independent, i.e., Φ and $\tilde{\Phi}$ are independent[1]. Since the α-GPP is stationary, without loss of generality we assume that the sensor node is located at the origin. Additionally, we assume that Φ is supported on a disk centered at the origin with radius R, that $\tilde{\Phi}$ is supported on a disk centered at the data sink with the same radius R. This latter assumption is also justified by the stationarity of the α-GPP.

Then, the harvested energy at the sensor node can be written as

$$P_H = \beta P_A \sum_{k \in \Phi} h_k d_k^{-l}, \tag{1}$$

where β presents the RF-to-DC power conversion efficiency, h_k is the fading gain of the channel between the sensor node and RF source k, d_k indicates the distance between the sensor node and ambient RF node k, and l represents the path loss exponent. Here, d_k can be represented as $d_k = \|\mathbf{x}_k\| + \epsilon$ where $\mathbf{x}_k \in \mathbb{R}^2$ and ϵ stand respectively for the coordinates of RF source node k and a fixed positive scalar which ensures that the harvested energy is finite in expectation (this can be checked by letting ϵ go to zero in Theorem 1). Note that when $\epsilon = 0$, there is a singularity at the origin ($\|\mathbf{x}_k\| = 0$). Also, assuming $\epsilon = 0$ is valid only for the far-field model and the effect of ϵ was analyzed in [37].

In the information transmission phase, by exploiting the harvested energy in (1), the sensor node transmits data to the data sink which is located at $\mathbf{x}_{ds} \in \mathbb{R}^2$. In practical systems, a base circuit power is consumed at the device [38]. Therefore, when we define P_{th} as the power required for the base circuit operation, the transmit power at the sensor node P_T can be expressed as

$$P_T = \begin{cases} 0 & \text{if } \ P_H < P_{\text{th}}, \\ P_H - P_{\text{th}} & \text{otherwise.} \end{cases} \tag{2}$$

Let us define W and σ^2 as the transmission bandwidth and the power of an additive white Gaussian noise (AWGN) at the

[1]The case where Φ and $\tilde{\Phi}$ are the same will be discussed in Appendix E.

data sink. Then, the maximum transmission rate at the data sink becomes

$$C = W\log_2\left(1+\frac{P_T h_0 d_0^{-l}}{\xi\left(\sum_{k\in\tilde{\Phi}} P_A \tilde{h}_k \tilde{d}_k^{-l}\right)+\sigma^2}\right), \quad (3)$$

where h_0 and $d_0 = \|\mathbf{x}_{ds}\|$ represent the fading power of the channel and the distance between the data sink and the sensor node, respectively. Also, $\tilde{h}_k$ and $\tilde{d}_k = \|\tilde{\mathbf{x}}_k - \mathbf{x}_{ds}\| + \epsilon$ are the fading gain of the channel and the distance between RF source k and the data sink, respectively, where $\tilde{\mathbf{x}}_k$ indicates the location of RF source k at the information transmission phase. Here, $\xi \in \{0,1\}$ is introduced to allow us to consider two different transmission scenarios, namely out-of-band transmission and in-band transmission. More precisely, when $\xi = 0$, the RF sources and the sensor node utilize different bands for their signal transmissions while they use the same band when $\xi = 1$. In other words, the signals transmitted by the RF sources are treated as interference at the data sink if $\xi = 1$.

The channel gains among the nodes in the networks are assumed to follow i.i.d. Nakagami-m distribution. Therefore, the distributions of fading gains can be expressed as $h_k \sim \mathcal{G}(m, \theta/m)$, $\tilde{h}_k \sim \mathcal{G}(m, \theta/m)$ and $h_0 \sim \mathcal{G}(m_0, \theta_0/m_0)$ where $\mathcal{G}(a,b)$ denotes the gamma distribution with shape parameter a and scale parameter b. Note that the Nakagami-m distribution includes the Rayleigh distribution as a special case ($m = 1$) and closely approximates the Rician distribution with Rician factor κ when m is set to $m = \frac{(1+\kappa)^2}{1+2\kappa}$. In addition, it is assumed that the fading gains $\{h_k\}$, $\{\tilde{h}_k\}$, h_0 and the α-GPPs are mutually independent.

In this paper, we focus on three important performance metrics, namely the mean of P_H, the power outage probability and the transmission outage probability. The power outage probability is the probability that the sensor node cannot scavenge power more than the base circuit power $P_{\rm th}$, and it can be computed as

$$\mathcal{P}_{\rm po} = \mathbb{P}\left(P_H < P_{\rm th}\right). \quad (4)$$

When the power outage occurs, the sensor node fails to send data to the data sink as the harvested energy is not sufficient to activate the circuit. Also, we define the transmission outage probability as the probability that the data rate in (3) is less than a certain threshold $C_{\rm th}$, and it can be written as

$$\mathcal{P}_{\rm to} = \mathbb{P}\left(C < C_{\rm th}\right). \quad (5)$$

The transmission outage can happen if the power outage occurs or the data rate at the sensor node is less than $C_{\rm th}$.

Note that, for the RF energy harvesting networks, upper bounds of $\mathcal{P}_{\rm po}$ and $\mathcal{P}_{\rm to}$ were introduced in [34] under the assumption that the fading channels are deterministic. In the next section, we will provide the fundamental properties of the DPP and the α-GPP, and derive new results on the α-GPP which allow us to derive exact expressions for the performance metrics.

III. Repulsive Point Process

In this section, we first address basic characteristics of the DPP and the α-GPP. Then, we introduce the Laplace transform of the α-GPP and a closed-form expression for the Fredholm determinant.

A. Determinantal point process

Let us consider a point process Φ on an observation window $O \subset \mathbb{R}^2$ with $0 \le |O| < \infty$ where $|O|$ indicates the Lebesgue measure of O. In other words, Φ is a finite random collection of points in O. In the theory of point processes [39] [40], the correlation functions $\lambda^{(n)}$ of Φ verify

$$\mathbb{E}\left[\prod_{i=1}^{n}\Phi(B_i)\right] = \int_{B_1\times\cdots\times B_n} \lambda^{(n)}(\mathbf{x}_1,\ldots,\mathbf{x}_n)\, d\mathbf{x}_1\ldots d\mathbf{x}_n,$$

for any family of mutually disjoint bounded subsets $B_i \subset \mathbb{R}^2$ for $i = 1,\ldots,n$. Here, $\lambda \triangleq \lambda^{(1)}$ denotes the spatial density of the point process Φ, and $\lambda^{(n)}(\mathbf{x}_1,\ldots,\mathbf{x}_n)\, d\mathbf{x}_1\ldots d\mathbf{x}_n$ means the probability of finding a point on Φ in the vicinity of each $\mathbf{x}_i \in \mathbb{R}^2$ for $i = 1,\ldots,n$.

We consider a map $K : \mathbb{C}^2 \mapsto \mathbb{C}$, and we assume in the following that K satisfies Condition A from [36], recalled below.

Hypothesis 1. *Denote by $\mathcal{K}$ the integral operator on $L^2(\mathbb{R}^2)$, the space of square integrable functions on $\mathbb{R}^2$, defined by*

$$\mathcal{K}f(\mathbf{x}) = \int_{\mathbb{R}^2} K(\mathbf{x},\mathbf{y}) f(\mathbf{y})\, d\mathbf{y}. \quad (6)$$

Assume that the map $\mathcal{K}$ is a Hilbert-Schmidt operator from $\mathrm{L}^2(\mathbb{R}^2)$ into $\mathrm{L}^2(\mathbb{R}^2)$ which satisfies the following conditions:

1) *the spectrum of $\mathcal{K}$ is included in $[0, -1/\alpha]$;*
2) *the map $\mathcal{K}$ is locally of trace-class (see e.g. [36] for a proper definition).*

The map K is called the *kernel* of the α-DPP. We let $\alpha = -1/j$ for a positive integer j. Then, a locally finite point process Φ on $\mathbb{R}^2$ is called an α-DPP with kernel K if its correlation functions $\lambda^{(n)}$ with respect to the Lebesgue measure exist and fulfill

$$\lambda^{(n)}(\mathbf{x}_1,\ldots,\mathbf{x}_n) = \det_\alpha\left(K(\mathbf{x}_i,\mathbf{x}_j)\right)_{1\le i,j\le n}, \quad (7)$$

where $\det_\alpha(\mathbf{A})$ represents the α-determinant of a matrix $\mathbf{A} = (\mathbf{A}_{i,j})_{1\le i,j\le n}$ [36] which can be computed as

$$\det_\alpha(\mathbf{A}) = \sum_{\sigma\in S_n} \alpha^{n-\nu(\sigma)} \prod_{i=1}^{n} \mathbf{A}_{i,\sigma(i)},$$

where S_n and $\nu(\sigma)$ indicate the n-th symmetric group and the number of cycles in the permutation $\sigma \in S_n$, respectively.

In the following propositions, we introduce fundamental properties of the α-DPP. We refer to [36] for mathematical details on the propositions.

Proposition 1. *For an α-DPP with kernel K, the covariance of the α-DPP is expressed as*

$$\mathrm{Cov}\left(N(A), N(B)\right) = \alpha \int_{A\times B} |K(\mathbf{x},\mathbf{y})|^2\, d\mathbf{x}d\mathbf{y},$$

where $A \subset \mathbb{R}^2$ and $B \subset \mathbb{R}^2$ are disjoint bounded sets, and $N(X)$ is the random number of point process points located within a bounded set $X \subset \mathbb{R}^2$.

The Fredholm determinant is a generalization of the determinant of a matrix and is defined for bounded operators on a Hilbert space. When $|\alpha| \leq 1$, the Fredholm determinant with a kernel K can be numerically evaluated as [36]

$$\begin{aligned} &\mathrm{Det}\left(I-\alpha K\right)^{-1/\alpha} \\ &= \sum_{n\geq 0} \frac{1}{n!} \int \det\nolimits_{\alpha}\left(K(\mathbf{x}_i,\mathbf{x}_j)\right)_{1\leq i,j\leq n} d\mathbf{x}_1 \ldots d\mathbf{x}_n. \end{aligned} \tag{8}$$

Proposition 2. *For an α-DPP Φ with kernel K and a bounded set A, the empty space function, i.e., hole probability, can be computed as*

$$\mathbb{P}\left(\Phi \cap A = \emptyset\right) = \mathrm{Det}\left(I+\alpha K_A\right)^{-1/\alpha}, \tag{9}$$

where $K_A(\mathbf{x},\mathbf{y}) = K(\mathbf{x},\mathbf{y})\mathbb{1}_A(\mathbf{x})\mathbb{1}_A(\mathbf{y})$ is the restriction of K to A^2, and $\mathbb{1}_A(\cdot)$ stands for the indicator function of a set A, i.e., $\mathbb{1}_A(\mathbf{x}) = 1$ for $\mathbf{x} \in A$ and $\mathbb{1}_A(\mathbf{x}) = 0$ for $\mathbf{x} \notin A$. Here, $\mathrm{Det}\left(I+\alpha K_A\right)^{-1/\alpha}$ has been defined in (8) *(simply replace K with $-K_A$).*

The α-DPPs have a closed-form Laplace transform which is expressed in terms of the Fredholm determinant.

Lemma 1 ([36], Theorem 1.2)**.** *For an α-DPP Φ with kernel K and a function $f : \mathbb{R}^2 \mapsto [0,+\infty)$, the Laplace transform of $\sum_{k\in\Phi} f(\mathbf{x}_k)$ is given by*

$$\mathbb{E}\left[\exp\left(-\sum_{k\in\Phi} f(\mathbf{x}_k)\right)\right] = \mathrm{Det}\left(I+\alpha K_f\right)^{-1/\alpha}, \tag{10}$$

where K_f is the kernel

$$K_f\left(\mathbf{x},\mathbf{y}\right) = \sqrt{1-\exp\left(-f(\mathbf{x})\right)} K\left(\mathbf{x},\mathbf{y}\right) \sqrt{1-\exp\left(-f(\mathbf{y})\right)}.$$

The Laplace transform of the received signal at a node plays an important role in analyzing the performance of wireless networks. Lemma 1 can be utilized to investigate networks where signals only suffer path loss attenuation which depends on the locations of the points in a point process. However, it is not applicable to networks where the received signal strength is determined by both the path loss and channel fading. In order to overcome this issue, in the following lemma we introduce a formula which provides the Laplace transform of the received signals which experience not only the path loss but also random channel fading.

Lemma 2. *Let us consider independent and identically distributed (i.i.d.) random variables $\{h_k\}_{k\in\mathbb{N}}$ which are independent from an α-DPP Φ. Then, for a function $f : \mathbb{R}^2 \mapsto [0,+\infty)$, the Laplace transform of $\sum_{k\in\Phi} h_k f(\mathbf{x}_k)$ becomes*

$$\mathbb{E}\left[\exp\left(-\sum_{k\in\Phi} h_k f(\mathbf{x}_k)\right)\right] = \mathrm{Det}\left(I+\alpha K_{h,f}\right)^{-1/\alpha}, \tag{11}$$

where $K_{h,f}$ is the kernel

$$K_{h,f}(\mathbf{x},\mathbf{y}) = \sqrt{1-M_h\left(-f(\mathbf{x})\right)} K\left(\mathbf{x},\mathbf{y}\right) \sqrt{1-M_h\left(-f(\mathbf{y})\right)},$$

$M_X(t) \triangleq \mathbb{E}\left[\exp\left(tX\right)\right]$ represents the moment generating function (MGF) of a random variable X, and $K\left(\mathbf{x},\mathbf{y}\right)$ is the kernel of the α-DPP Φ. Note that both (10) and (11) are expressed in terms of the Fredholm determinant, and therefore the complexity orders for evaluating (10) and (11) are the same.

Proof. Since $\{h_k\}$ and Φ are independent,

$$\begin{aligned} &\mathbb{E}\left[\exp\left(-\sum_{k\in\Phi} h_k f(\mathbf{x}_k)\right)\right] \\ &= \mathbb{E}\left[\prod_{k\in\Phi} \mathbb{E}\left[\exp\left(-h_k f(\mathbf{x}_k)\right)\right]\right] \\ &= \mathbb{E}\left[\prod_{k\in\Phi} M_h\left(-f(\mathbf{x}_k)\right)\right] \\ &= \mathbb{E}\left[\exp\left(\sum_{k\in\Phi} \ln\left(M_h\left(-f(\mathbf{x}_k)\right)\right)\right)\right] \\ &\overset{(a)}{=} \mathrm{Det}\left(I+\alpha K_{h,f}\right)^{-1/\alpha}, \end{aligned}$$

where $\ln(x)$ is the natural logarithm function, and (a) follows from Lemma 1. □

B. α-Ginibre point process

Now, we focus on the α-GPP and set the observation window O to $O = \mathcal{B}_{\mathbf{o}}(R)$. The α-GPP is the α-DPP defined by the Ginibre kernel which is given by

$$K\left(\mathbf{x},\mathbf{y}\right) = \lambda \exp\left(\pi\lambda \mathbf{x}\bar{\mathbf{y}} - \frac{\pi\lambda}{2}\left(\|\mathbf{x}\|^2 + \|\mathbf{y}\|^2\right)\right), \tag{12}$$

for $\mathbf{x} \in \mathcal{B}_0(R)$ and $\mathbf{y} \in \mathcal{B}_0(R)$, where λ is the spatial density of the α-GPP. In the remainder of the paper, K shall denote the Ginibre kernel (12). Note that the Ginibre kernel is identical to the Ginibre kernel defined in [41], except for the fact that we have introduced a spatial density parameter allowing us to adjust the RF sources density. Also, the distribution of the α-GPP is invariant under rotations and translations since by property the α-GPP is stationary and isotropic. In addition, as K is a Hermitian compact operator, from the spectral theorem, $K\left(\mathbf{x},\mathbf{y}\right)$ can be represented as $K\left(\mathbf{x},\mathbf{y}\right) = \sum_{n\geq 0} \rho_n \phi_n(\mathbf{x})\overline{\phi_n(\mathbf{y})}$ where $\{\phi_n(\mathbf{x})\}$ and $\{\rho_n\}$ account for basis of eigenvectors of $\mathrm{L}^2(\mathcal{B}_{\mathbf{o}}(R))$ and the corresponding eigenvalues, respectively. Here, we can compute ρ_n and $\phi_n(\mathbf{x})$ as [41]

$$\rho_n = \frac{\gamma\left(n+1, \pi\lambda R^2\right)}{n!},$$

and

$$\phi_n(\mathbf{x}) = \sqrt{\frac{\lambda}{n!\rho_n}} \left(\sqrt{\pi\lambda}\mathbf{x}\right)^n \exp\left(-\frac{\pi\lambda}{2}\|\mathbf{x}\|^2\right),$$

where $\gamma(a,b) \triangleq \int_0^b t^{a-1}e^{-t}dt$ is the lower incomplete gamma function.

As can be seen in (9), (10) and (11), many important characteristics of the α-DPP – and thus also the α-GPP – are given in terms of the Fredholm determinant which can be

computed by (8). However, the determinants in (8) may incur a high computational complexity. In the following lemma, we introduce a simple closed-form expression for the Fredholm determinant when the kernel is related to the Ginibre kernel by (13).

Lemma 3. *Let us define K_q as*

$$K_q(\mathbf{x},\mathbf{y}) = q(\|\mathbf{x}\|)K(\mathbf{x},\mathbf{y})q(\|\mathbf{y}\|), \tag{13}$$

where $q:[0,\infty)\to\mathbb{R}$ is a function such that $\mathrm{Det}(I+\alpha K_q)$ is well defined and K is given by (12)*. Then, the Fredholm determinant $\mathrm{Det}(I+\alpha K_q)$ can be expressed as*

$$\mathrm{Det}(I+\alpha K_q) = \prod_{n\geq 0}\left(1+\frac{2\alpha\left(\pi\lambda\right)^{n+1}}{n!}\right. \times \left.\int_0^R q(r)^2\exp\left(-\pi\lambda r^2\right) r^{2n+1}\,dr\right). \tag{14}$$

Proof. See Appendix A. □

The usual approach to evaluate the Fredholm determinant follows the techniques from [42] and consists in approximating (8) by the determinant of an $N_{\mathrm{det}}\times N_{\mathrm{det}}$ matrix. The complexity of this approach is thus in $\mathcal{O}(N_{\mathrm{det}}^3)$. Defining instead $\Upsilon_{N_{\mathrm{closed}}}$ as the truncated product from (14), i.e.,

$$\Upsilon_{N_{\mathrm{closed}}} = \prod_{n=0}^{N_{\mathrm{closed}}}\left(1+\frac{2\alpha\left(\pi\lambda\right)^{n+1}}{n!}\right. \times \left.\int_0^R q(r)^2\exp\left(-\pi\lambda r^2\right) r^{2n+1}\,dr\right), \tag{15}$$

the complexity in computing $\Upsilon_{N_{\mathrm{closed}}}$ is $\mathcal{O}(N_{\mathrm{closed}})$. We note that the usual method for the computation of (8) exhibits a polynomial rate of convergence to the true value of the Fredholm determinant, while the truncation (15) convergences exponentially fast, see [42]. The exponential convergence rate of (15) as N_{closed} goes to infinity follows from the smoothness of the kernel of the Ginibre point process. Hence, the closed-form expression in (14) allows us to evaluate the Fredholm determinant with a significantly reduced complexity.

We conclude this section by recalling a difference between the α-GPP and the PPP. Letting $A\subset\mathbb{R}^2$ and $B\subset\mathbb{R}^2$ be two disjoint bounded sets and plugging the Ginibre Kernel in (12) into Proposition 1, we have

$$\mathrm{Cov}(N(A),N(B)) = \alpha\lambda^2\int_{A\times B} e^{-\pi\lambda\|\mathbf{x}-\mathbf{y}\|^2}\,\mathrm{d}\mathbf{x}\mathrm{d}\mathbf{y} \leq 0,$$

which contrasts with the PPP for which the above covariance is zero. Indeed, in a PPP, the location of a point does not depend on the positions of the others. The interpretation of the above equation is that, contrary to the PPP setting, the numbers of points in two disjoint sets are negatively correlated since $\alpha<0$. This leads to the α-GPP being more spread-out and exhibiting less clustering than a PPP.

Until now, we have investigated the fundamental characteristics of the α-DPP and the α-GPP. Also, we have introduced the new Lemmas 2 and 3 on the α-DPP and α-GPP, respectively. Next, we will analyze the performance of the ambient RF energy harvesting wireless sensor networks, i.e., the mean of P_H, $\mathcal{P}_{\mathrm{po}}$, $\mathcal{P}_{\mathrm{to}}$ and an upper bound of $\mathcal{P}_{\mathrm{po}}$.

IV. Performance Analysis

In this section, we provide semi-closed-form expressions for the performance metrics. First, we concentrate on the mean of the harvested energy, and then we move on to the power outage and transmission outage probabilities.

A. Mean of the harvested energy

By exploiting Campbell's theorem [43][2], we can derive the mean of the harvested energy P_H as illustrated in the following theorem.

Theorem 1. *The mean of P_H in (1) is given by*

$$\mathbb{E}\left[P_H\right] = \begin{cases} 2\pi\beta\theta\lambda P_A\left(\ln\left(1+\frac{R}{\epsilon}\right)-\frac{R}{R+\epsilon}\right) & \text{if } l=2,\\ 2\pi\beta\theta\lambda P_A\left(R-\epsilon\ln\left(1+\frac{R}{\epsilon}\right)\right) & \text{if } l=1,\\ \frac{2\pi\beta\theta\lambda P_A\left(\epsilon^{2-l}-(R+\epsilon)^{1-l}(\epsilon+(l-1)R)\right)}{(l-2)(l-1)} & \text{otherwise.}\end{cases} \tag{16}$$

Proof. Due to the independence of the fading gains $\{h_k\}$ and the α-GPP Φ, we have

$$\begin{aligned}\mathbb{E}\left[P_H\right] &= \beta P_A\mathbb{E}\left[\sum_{k\in\Phi}\mathbb{E}\left[h_k\right]d_k^{-l}\right] = \beta\theta P_A\mathbb{E}\left[\sum_{k\in\Phi}d_k^{-l}\right]\\ &\overset{(b)}{=} \beta\theta P_A\int_{\mathcal{B}_0(R)} d_k^{-l}\lambda^{(1)}(\mathbf{x})\,d\mathbf{x}\\ &= \beta\theta\lambda P_A\int_{\mathcal{B}_0(R)}\left(\|\mathbf{x}\|+\epsilon\right)^{-l}\,d\mathbf{x}\\ &\overset{(c)}{=} 2\pi\beta\theta\lambda P_A\int_0^R\frac{r}{(r+\epsilon)^l}\,dr,\end{aligned}$$

where $\lambda^{(1)}(\mathbf{x})$ denotes the first correlation function (cf. (7)), and (b) and (c) follow from Campbell's theorem and a polar change of variables, respectively. In addition, after some manipulations, the integral in the above equation can be computed in a closed-form and (16) follows. □

From (16), we note that the mean of P_H linearly increases as the parameters β,θ,λ and P_A become larger. Note that R determines the size of the observation window, and therefore a growth of R results in an increase of the number of RF sources. Hence, the mean of P_H increases when R grows as observed in (16). Also, as expected, $\mathbb{E}\left[P_H\right]$ is a decreasing function of ϵ. It is important to remark that $\mathbb{E}\left[P_H\right]$ is not influenced by the scattering parameter α. This is due to the fact that α-GPP is a stationary point process. Therefore, the means of P_H for the cases of α-GPP and PPP are identical when the point processes have the same spatial density.

B. Power outage probability

In this subsection, we introduce new semi-closed-form expressions for the power outage probability defined in (4), as well as some simpler upper-bounds. Before stating our results, we recall Mellin's formula for the computation of the inverse

[2]For a point process Ψ with density λ and a function $f:\mathbb{R}^2\mapsto\mathbb{R}$, the mean of the random sum $\sum_{k\in\Psi}f(k)$ is equal to $\int_{\mathbb{R}^2}f(\mathbf{x})\lambda(\mathbf{x})\,\mathrm{d}\mathbf{x}$.

Laplace transform. Namely, for a fixed real-valued function F, we define

$$\mathcal{L}^{-1}\{F\}(x) \triangleq \frac{1}{2\pi i}\lim_{T\to\infty}\int_{c-iT}^{c+iT}\exp(sx)F(s)\,ds, \quad x\in\mathbb{R},$$

where c is a fixed constant greater than the real parts of the singularities of F and $i \triangleq \sqrt{-1}$ represents the imaginary unit. First, we focus on the exact power outage probability which will be derived in the following theorem.

Theorem 2. *When the harvested energy at the sensor node is defined as in (1), we can express the exact power outage probability as*

$$\mathcal{P}_{\rm po} = F_{P_H}(P_{\rm th}), \tag{17}$$

where $F_{P_H}(x)$ is the cumulative distribution function (CDF) of P_H which is given by

$$F_{P_H}(x) = \mathcal{L}^{-1}\left\{\frac{1}{s}\,\mathrm{Det}\left(I+\alpha A_s\right)^{-1/\alpha}\right\}(x). \tag{18}$$

Here, A_s is the kernel given by

$$\begin{aligned} A_s(\mathbf{x},\mathbf{y}) =& \sqrt{1-\left(1+\frac{s\beta\theta P_A}{m(||\mathbf{x}||+\epsilon)^l}\right)^{-m}} \\ &\times K(\mathbf{x},\mathbf{y})\sqrt{1-\left(1+\frac{s\beta\theta P_A}{m(||\mathbf{y}||+\epsilon)^l}\right)^{-m}}, \end{aligned} \tag{19}$$

when $h_k \sim \mathcal{G}(m,\theta/m)$, and

$$\begin{aligned} A_s(\mathbf{x},\mathbf{y}) =& \sqrt{1-\exp\left(-\frac{s\beta\theta P_A}{(||\mathbf{x}||+\epsilon)^l}\right)} \\ &\times K(\mathbf{x},\mathbf{y})\sqrt{1-\exp\left(-\frac{s\beta\theta P_A}{(||\mathbf{y}||+\epsilon)^l}\right)}, \end{aligned} \tag{20}$$

when there is no fading, i.e., h_k is constant equal to θ for all k. In both of the above equations, K is the Ginibre kernel defined in (12)*. Additionally, the PDF of P_H, denoted by $f_{P_H}(x)$, is computed as*

$$f_{P_H}(x) = \mathcal{L}^{-1}\left\{\mathrm{Det}\left(I+\alpha A_s\right)^{-1/\alpha}\right\}(x). \tag{21}$$

Proof. See Appendix B. □

Note that the inverse Laplace transforms in (18) and (21) can be easily evaluated by using modern tools such as the algorithm presented in [44]. Moreover, we can easily compute the Fredholm determinants in Theorem 2 by applying Lemma 3.

We also note that the result proved in Theorem 2 recovers the PPP setting by letting α tend to zero. Indeed, using the expansion[3] [36]

$$\mathrm{Det}\left(I+\alpha A_s\right) = 1+\alpha\int_{\mathcal{B}_{\mathbf{o}}(R)} A_s(\mathbf{x},\mathbf{x})\,d\mathbf{x} + O_{\alpha\to 0}(\alpha^2),$$

it is readily proved that

$$\mathrm{Det}\left(I+\alpha A_s\right)^{-1/\alpha} \xrightarrow[\alpha\to 0]{} \exp\left(-\int_{\mathcal{B}_{\mathbf{o}}(R)} A_s(\mathbf{x},\mathbf{x})\,d\mathbf{x}\right).$$

[3]Here, we say that $f = O_{\alpha\to 0}(g)$ if there exists a positive constant M such that $|f(\alpha)| \le M|g(\alpha)|$ as α goes to zero.

Focusing on the Rayleigh-fading case (obtained by plugging $m=1$ into (19)), for PPPs, using Theorem 2 and a polar change of variables recovers the formula

$$\begin{aligned} &\mathcal{P}_{\rm po} \\ &= \mathcal{L}^{-1}\left\{\frac{1}{s}\exp\left(-2\pi\lambda\int_0^R \frac{r}{1+(r+\epsilon)^{\ell}(s\beta\theta P_A)^{-1}}dr\right)\right\}(P_{\rm th}), \end{aligned}$$

obtained in [17] (cf. equation (6) therein). This expression has been further simplified in [17], as shown in the next corollary obtained when $\epsilon=0$, $\theta=1$ and $R\to\infty$.

Corollary 1 ([17])**.** *When Φ is a PPP with a density λ, the power outage probability becomes*

$$\begin{aligned} \mathcal{P}_{\rm po} = 1 - \int_0^\infty \frac{1}{\pi u}\exp\left(-uP_{\rm th} - \frac{2\pi^2\lambda(\beta P_A u)^{2/l}}{l\tan(2\pi/l)}\right) \\ \times \sin\left(\frac{2\pi^2\lambda(\beta P_A u)^{2/l}}{l}\right)du. \end{aligned}$$

Furthermore, when $l=4$, $\mathcal{P}_{\rm po}$ and the PDF of P_H can be respectively expressed as

$$\mathcal{P}_{\rm po} = 1-\mathrm{erf}\left(\frac{\pi^2\lambda}{4}\sqrt{\frac{\beta P_A}{P_{\rm th}}}\right), \quad \textit{and}$$

$$f_{P_H}(x) = \frac{\pi^2\lambda}{4}\sqrt{\frac{\beta P_A}{\pi x^3}}\exp\left(-\frac{\pi^4\lambda^2\beta P_A}{16x}\right),$$

where $\mathrm{erf}(x) \triangleq \frac{2}{\sqrt{\pi}}\int_0^x \exp(-t^2)\,dt$ denotes the error function.

Note that although the results in Theorem 2 accurately predict the power outage probability and enable us to evaluate the power outage probability with substantially reduced simulation time compared to the Monte Carlo simulations, the computational complexity can be further reduced when the inverse Laplace transforms is not employed. To that aim, we focus on providing upper bounds on the power outage probability $\mathcal{P}_{\rm po}$ which do not require the inverse Laplace transform operation.

In [34], an upper bound of $\mathcal{P}_{\rm po}$ was derived under the assumption that the fading gains are constant. In the following theorem, we introduce a new expression for an upper bound $\mathcal{P}_{\rm po}$ in networks with Nakagami-m distributed fading channels.

Theorem 3. *When $h_k \sim \mathcal{G}(m,\theta/m)$, an upper bound of $\mathcal{P}_{\rm po}$ in (4) can be obtained as*

$$\mathcal{P}_{\rm po} \le \mathrm{Det}\left(I+\alpha B\right)^{-1/\alpha}, \tag{22}$$

where B is the kernel

$$\begin{aligned} B(\mathbf{x},\mathbf{y}) =& \sqrt{1-\frac{\gamma\left(m,\frac{mP_{\rm th}(||\mathbf{x}||+\epsilon)^l}{\beta\theta P_A}\right)}{\Gamma(m)}} \\ &\times K(\mathbf{x},\mathbf{y})\sqrt{1-\frac{\gamma\left(m,\frac{mP_{\rm th}(||\mathbf{y}||+\epsilon)^l}{\beta\theta P_A}\right)}{\Gamma(m)}}, \end{aligned}$$

where K is defined in (12) *and $\Gamma(t)=\int_0^\infty x^{t-1}\exp(-x)dx$ is the gamma function.*

Proof. See Appendix C. □

For networks with constant fading channels $h_k = \theta, \forall k$, we recall in the next corollary an upper bound of $\mathcal{P}_{\rm po}$ which has been obtained in [34] by similar arguments.

Corollary 2 ([34])**.** *When $h_k = \theta,\ \forall k$, an upper bound of $\mathcal{P}_{\rm to}$ is given by*

$$\mathcal{P}_{\rm po} \leq \mathrm{Det}\left(I + \alpha K_{\mathcal{B}_{\mathbf{o}}(\min(R,c_1))}\right)^{-1/\alpha},$$

where $c_1 \triangleq \left(\frac{\beta\theta P_A}{P_{\rm th}}\right)^{1/l} - \epsilon$.

We remark again that the Fredholm determinants in Theorem 3 and Corollary 2 are evaluated by applying Lemma 3, and thus the complexity orders of the results in Theorem 3 and Corollary 2 are the same. The advantage of the bounds in Theorem 3 and Corollary 2 is that they can be computed faster than the exact formula from Theorem 2 which involves the inverse Laplace transform. In Section V, the tightness of the bounds will be examined and it will be shown that the bounds exhibit the same trend as the exact power outage probability.

Until now, we have derived semi-closed-form expressions for the exact and upper bound of power outage probability. Since the transmission rate C is directly related to P_H via (2) and (3), identifying the characteristics of P_H is necessary in order to investigate the transmission outage probability $\mathcal{P}_{\rm to}$ defined in (5). In the next subsection, we will examine $\mathcal{P}_{\rm to}$ based on the CDF and the PDF of P_H derived in Theorem 2.

C. Transmission outage probability

In this subsection, we derive exact analytical expressions for the transmission outage probability $\mathcal{P}_{\rm to}$ defined in (5). First, we can calculate $\mathcal{P}_{\rm to}$ by

$$\begin{aligned}\mathcal{P}_{\rm to} &= \mathbb{P}\left(C < C_{\rm th}\right)\\ &= \mathbb{P}\left(C < C_{\rm th}, P_H < P_{\rm th}\right) + \mathbb{P}\left(C < C_{\rm th}, P_H \geq P_{\rm th}\right)\\ &\overset{\rm (d)}{=} \mathbb{P}\left(P_H < P_{\rm th}\right) + \mathbb{P}\left(C < C_{\rm th}, P_H \geq P_{\rm th}\right)\\ &= \mathbb{P}\left(P_H < P_{\rm th}\right) + \tilde{\mathcal{P}}_{\rm to}, \end{aligned} \tag{23}$$

where we define $\tilde{\mathcal{P}}_{\rm to}$ as

$$\tilde{\mathcal{P}}_{\rm to} = \mathbb{P}\left(\frac{P_T h_0 d_0^{-l}}{\xi Q + \sigma^2} < \eta, P_H \geq P_{\rm th}\right), \tag{24}$$

where $\eta \triangleq 2^{C_{\rm th}/W} - 1$, and $Q \triangleq \sum_{k\in\tilde{\Phi}} P_A \tilde{h}_k \tilde{d}_k^{-l}$ denotes the interference at the data sink. Here, (d) follows from the fact that C is always less than $C_{\rm th}$ when $P_H \leq P_{\rm th}$ since the transmit power P_T is equal to zero when $P_H \leq P_{\rm th}$ as seen in (2). Note that, as shown in (23), $\mathcal{P}_{\rm to}$ is the sum of two probabilities, namely the power outage probability $\mathcal{P}_{\rm po}$ and the probability that the data transmission rate with transmit power P_T is smaller than $C_{\rm th}$ when $P_T \geq 0$ ($P_H \geq P_{\rm th}$), respectively.

First, we consider the case where the fading channel between the sensor node and the data sink follows the Rayleigh fading, i.e., $m_0 = 1$. In this case, h_0 follows the exponential distribution $\mathcal{E}(1/\theta_0)$ where $\mathcal{E}(a)$ denotes the exponential distribution with parameter a. In the following theorem, by using the obtained PDF of P_H, we introduce a semi-closed-form expression for transmission outage probability $\mathcal{P}_{\rm to}$.

Theorem 4. *When $h_k \sim \mathcal{G}\left(m, \theta/m\right)$, $\tilde{h}_k \sim \mathcal{G}\left(m, \theta/m\right)$ and $h_0 \sim \mathcal{E}(1/\theta_0)$, $\mathcal{P}_{\rm to}$ is given by*

$$\begin{aligned}\mathcal{P}_{\rm to} = 1 - \int_{P_{\rm th}}^{\infty} &\exp\left(-\frac{\eta d_0^l \sigma^2}{\theta_0\left(x - P_{\rm th}\right)}\right)\\ &\times \mathrm{Det}\left(I + \alpha C_x\right)^{-1/\alpha} f_{P_H}(x)\, dx,\end{aligned} \tag{25}$$

where $f_{P_H}(x)$ is the PDF of the harvested energy at the sensor node in (21) and C_x is the kernel

$$\begin{aligned}C_x(\mathbf{x},\mathbf{y}) = &\sqrt{1 - \left(1 + \frac{\theta\eta d_0^l \xi P_A}{m\theta_0(x - P_{\rm th})(||\mathbf{x}|| + \epsilon)^l}\right)^{-m}}\\ &\times K(\mathbf{x},\mathbf{y})\sqrt{1 - \left(1 + \frac{\theta\eta d_0^l \xi P_A}{m\theta_0(x - P_{\rm th})(||\mathbf{y}|| + \epsilon)^l}\right)^{-m}},\end{aligned} \tag{26}$$

where K is the Ginibre kernel defined in (12)*. If the out-of-band transmission is employed ($\xi = 0$), $\mathcal{P}_{\rm to}$ in (25) is simplified as*

$$\mathcal{P}_{\rm to} = 1 - \int_{P_{\rm th}}^{\infty} \exp\left(-\frac{\eta d_0^l \sigma^2}{\theta_0\left(x - P_{\rm th}\right)}\right) f_{P_H}(x)\, dx.$$

Proof. See Appendix D. □

In Theorem 4, we have assumed that the locations of the RF sources in the energy harvesting and information transmission phases by Φ and $\tilde{\Phi}$ are independent. We remark that one can also assume that they are the same point process, but this comes at the cost of computational complexity. We provide an explicit expression of $\mathcal{P}_{\rm to}$ in this setting in Appendix E.

In the following theorem, we extend the result of Theorem 4 by assuming that the channel between the sensor node and the data sink undergoes Nakagami fading instead of Rayleigh fading. More specifically, we provide an explicit analytical representation for the transmission outage probability when h_0 is modeled as the Gamma random variable with positive integer parameter m_0.

Theorem 5. *When $h_k \sim \mathcal{G}\left(m, \theta/m\right)$, $\tilde{h}_k \sim \mathcal{G}\left(m, \theta/m\right)$ and $h_0 \sim \mathcal{G}\left(m_0, \theta_0/m_0\right)$, $\mathcal{P}_{\rm to}$ can be expressed as*

$$\begin{aligned}\mathcal{P}_{\rm to} = 1 - \lim_{\tau\to 0} &\sum_{i=0}^{m_0-1}\sum_{j=0}^{i} \frac{1}{i!}\binom{i}{j}\left(\frac{m_0}{\theta_0\tau}\right)^i (-1)^j\\ &\times \int_{P_{\rm th}}^{\infty}\left(\frac{\eta d_0^l}{x - P_{\rm th}}\right)^i \mathrm{Det}\left(I + \alpha D_{(\mu_x + \tau(j - i/2))\xi P_A}\right)^{-1/\alpha}\\ &\times \exp(-(\mu_x + \tau(j - i/2))\sigma^2) f_{P_H}(x)\, dx,\end{aligned} \tag{27}$$

where $\mu_x \triangleq \frac{m_0\eta d_0^l}{\theta_0(x - P_{\rm th})}$ and D_s is the kernel

$$\begin{aligned}D_s(\mathbf{x},\mathbf{y}) = &\sqrt{1 - \left(1 + \frac{s\theta}{m(||\mathbf{x}|| + \epsilon)^l}\right)^{-m}}\\ &\times K(\mathbf{x},\mathbf{y})\sqrt{1 - \left(1 + \frac{s\theta}{m(||\mathbf{y}|| + \epsilon)^l}\right)^{-m}},\end{aligned} \tag{28}$$

where K is the Ginibre kernel defined in (12)*. Also, when $\xi = 0$, $\mathcal{P}_{\rm to}$ in (27) can be simplified as*

$$\mathcal{P}_{\rm to} = 1 - \sum_{i=0}^{m_0-1} \frac{1}{i!} \left(\frac{m_0 \eta d_0^l \sigma^2}{\theta_0} \right)^i \times \int_{P_{\rm th}}^{\infty} \left(\frac{1}{x - P_{\rm th}} \right)^i \exp\left(- \frac{m_0 \eta d_0^l \sigma^2}{\theta_0 (x - P_{\rm th})} \right) f_{P_H}(x)\, dx.$$

Proof. See Appendix F. □

In addition, we derive an expression for the transmission outage probability in networks with constant fading in the following theorem.

Theorem 6. *When the fading channels are constant as $h_k = \tilde{h}_k = \theta$, $\forall k$ and $h_0 = \theta_0$, the transmission outage probability $\mathcal{P}_{\rm to}$ becomes*

$$\mathcal{P}_{\rm to} = 1 - \int_{c_2}^{\infty} F_Q \left(\frac{\theta_0 (x - P_{\rm th})}{\eta d_0^l} - \sigma^2 \right) f_{P_H}(x)\, dx, \quad (29)$$

where $c_2 = P_{\rm th} + \frac{\eta d_0^l \sigma^2}{\theta_0}$, $F_Q(x)$ is the CDF of Q which is computed as

$$F_Q(x) = \mathcal{L}^{-1} \left\{ \mathrm{Det}\left(I + \alpha E_s \right)^{-1/\alpha} \right\},$$

and E_s is the kernel

$$E_s(\mathbf{x}, \mathbf{y}) = \sqrt{1 - \exp\left(- \frac{s\theta P_A}{(||\mathbf{x}|| + \epsilon)^l} \right)} \times K(\mathbf{x}, \mathbf{y}) \sqrt{1 - \exp\left(- \frac{s\theta P_A}{(||\mathbf{y}|| + \epsilon)^l} \right)}, \quad (30)$$

where K is the Ginibre kernel defined in (12)*. Additionally, when $\xi = 0$, $\mathcal{P}_{\rm to}$ is expressed as*

$$\mathcal{P}_{\rm to} = F_{P_H} \left(P_{\rm th} + \frac{\eta \sigma^2 d_0^l}{\theta_0} \right). \quad (31)$$

Proof. See Appendix G. □

In equation (29), we see that the term $\theta_0 (x - P_{\rm th}) (\eta d_0^l)^{-1} - \sigma^2$ is an increasing (respectively a decreasing) function of θ_0 (respectively $P_{\rm th}$, $C_{\rm th}$, d_0 and σ^2) since $\eta = 2^{C_{\rm th}/W} - 1$. Also, c_2 decreases as θ_0 (respectively $P_{\rm th}$, $C_{\rm th}$, d_0 and σ^2) becomes larger (respectively smaller). Therefore, it is expected that $\mathcal{P}_{\rm to}$ in (29) grows as θ_0 (respectively $P_{\rm th}$, $C_{\rm th}$, d_0 and σ^2) decreases (respectively increases). The same observation can be made for the out-of-band transmission case in (31). Lastly, we mention that the Fredholm determinants in Theorems 4 to 6 can be computed by Lemma 3.

V. Simulation Results

In this section, we present numerical results to validate our analytical results, under the assumption that h_0, $\{h_k\}$ and $\{\tilde{h}_k\}$ follow Nakagami-m distribution. We assume $\theta = \theta_0 = 1$ and $l = 4$. The transmit power of ambient RF sources P_A is set to $P_A = 0.1$ W which is within the normal transmit power of cellular mobiles. Also, the base circuit power $P_{\rm th}$ is $P_{\rm th} = -18$ dBm (i.e., 15.8 μW) [6], the bandwidth of the transmitted signal W is $W = 20$ MHz, and noise power at the data sink is white Gaussian with power spectral density -120 dBm/Hz [45]. The RF-to-DC power conversion efficiency is assumed to be $\beta = 0.25$, $\epsilon = 0.05$, $R = 30$, and the centers of the GPPs Φ and $\tilde{\Phi}$ are the origin and $\mathbf{x}_{ds}$, respectively. In addition, we evaluate the Fredholm determinant by using (15) and set $N_{\rm closed}$ as $N_{\rm closed} = 100$.[4] Unless otherwise stated, we set the simulation parameters as listed in Table I .

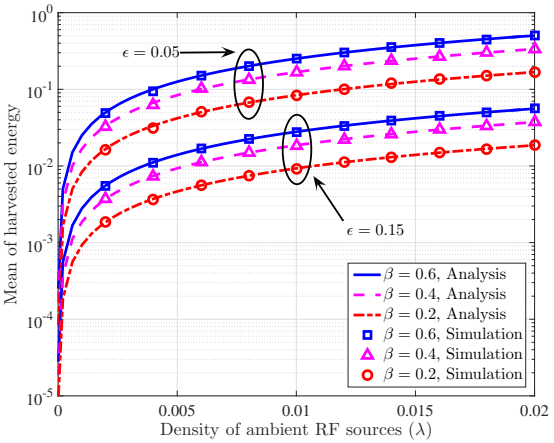

Fig. 3. Mean of harvested energy $\mathbb{E}[P_H]$ as a function of λ

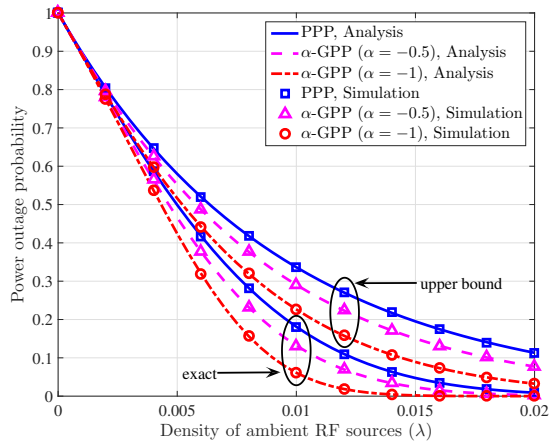

Fig. 4. Power outage probability $\mathcal{P}_{\rm po}$ as a function of λ

In the sequel, we use the lines and symbols to indicate the analytical and simulated results, respectively. In Fig. 3, the mean of harvested energy is presented as a function of λ with various values of β and ϵ. We see that the analytical result in (16) is accurate and matches the simulated results. As expected, the mean of the harvested energy increases as the density of RF sources and the RF-to-DC power conversion efficiency β become larger. Also, as the minimum distance between the sensor node and the RF sources ϵ decreases, the mean of the harvested energy grows, since the smaller distance between the sensor node and the ambient RF sources leads to the larger received power.

[4] We have confirmed from computer simulations that $\Upsilon_{N_{\rm closed}}$ in (15) with $N_{\rm closed}$ larger than 100 has a negligible impact.

TABLE I
SYSTEM PARAMETERS

Symbol	θ	θ_0	m	m_0	l	P_A	P_{th}	W	σ^2	β	ϵ	α	R
Value	1	1	1	1	4	0.1 W	15.8 μW	20 MHz	-120 dBm/Hz	25 %	0.05m	-1	30m

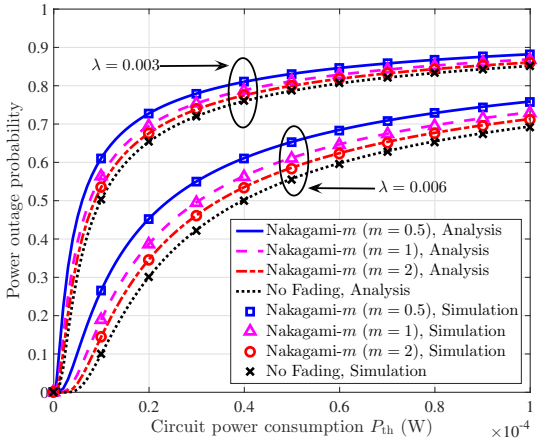

Fig. 5. Power outage probability $\mathcal{P}_{\text{po}}$ as a function of P_{th}

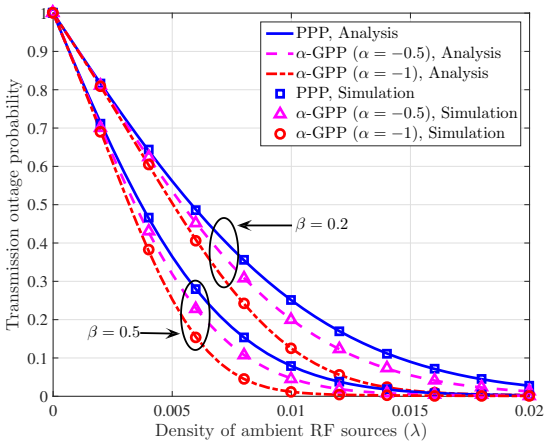

Fig. 7. Transmission outage probability $\mathcal{P}_{\text{to}}$ as a function of λ ($d_0 = 10, C_{\text{th}} = 0.05$ and $\xi = 0$)

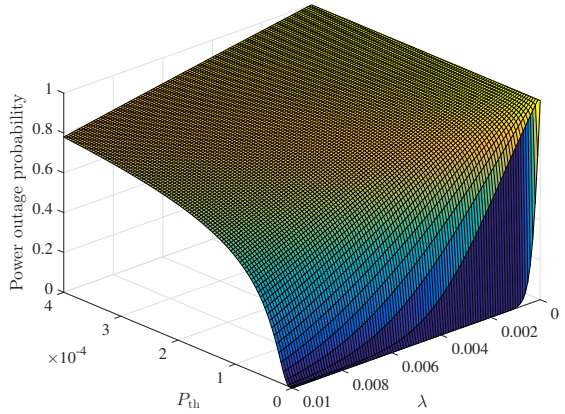

Fig. 6. Power outage probability $\mathcal{P}_{\text{po}}$ as functions of λ and P_{th}

Fig. 4 demonstrates the exact and upper bounds of power outage probability $\mathcal{P}_{\text{po}}$ in networks with α-GPP and PPP distributed ambient RF sources. Here, we obtain the analytical results for the upper bound using (22), and the simulation results for the upper bound by evaluating the probability $\mathbb{P}(\forall k \in \Phi, h_k d_k^{-l} < \frac{P_{\text{th}}}{\beta P_A})$ in (34) by Monte-Carlo simulation. It is observed that $\mathcal{P}_{\text{po}}$ is a monotonically decreasing function of the density λ, and the impact of λ is more pronounced when λ is small. Also, we see that the exact and the upper bounds of $\mathcal{P}_{\text{po}}$ exhibit the same trend.

In Fig. 5, we illustrate the power outage probability as a function of P_{th} in the cases of $\lambda = 0.003$ and 0.006. As can be seen from Fig. 5, $\mathcal{P}_{\text{po}}$ tends to grow almost logarithmically with the increase of P_{th}. In other words, when P_{th} is small, $\mathcal{P}_{\text{po}}$ varies more dynamically with a change of P_{th} than when P_{th} is large. If $m < 1$ (respectively $m > 1$), the fading is more (respectively less) severe than the Rayleigh fading ($m = 1$), and the fading channel becomes constant (no fading) when $m \to \infty$. Hence, $\mathcal{P}_{\text{po}}$ grows as m decreases since the harvested energy is directly related to the power of the fading channel. In addition, we can observe that $\mathcal{P}_{\text{po}}$ is more susceptible to m when λ is large.

Fig. 6 presents the influence of λ and P_{th} on the power outage probability. It is seen that $\mathcal{P}_{\text{po}}$ is a monotonically decreasing (respectively increasing) function of λ (respectively P_{th}) regardless of P_{th} (respectively λ). Also, we observe that λ has more impact on $\mathcal{P}_{\text{po}}$ when P_{th} is small. That is to say, when P_{th} is relatively large, $\mathcal{P}_{\text{po}}$ slowly (almost linearly) degrades as λ becomes larger while $\mathcal{P}_{\text{po}}$ rapidly decreases as λ increases when P_{th} is small. Moreover, we see that $\mathcal{P}_{\text{po}}$ is significantly affected by λ and P_{th} if λ and P_{th} are close to 0.

In Figs. 7, 8 and 9, we show the transmission outage probabilities $\mathcal{P}_{\text{to}}$ as a function of λ for both scenarios of out-of-band ($\xi = 0$) and in-band ($\xi = 1$) transmissions. For all cases, $\mathcal{P}_{\text{to}}$ decreases as β increases. The reason is straightforward as the higher β makes the transmit power at the sensor larger. In addition, as expected, $\mathcal{P}_{\text{to}}$ is a non-increasing function of the density λ. However, unlike the out-of-band transmission case ($\xi = 0$), for the in-band transmission ($\xi = 1$), $\mathcal{P}_{\text{to}}$ is saturated as λ grows. This is due to the fact that a growth of λ increases not only the harvested energy at the sensor node but also the interference at the data sink. From the observation that $\mathcal{P}_{\text{to}}$ decreases as λ increases when λ is small, we can infer that the transmission outage is mainly caused by the power outage at the sensor node when λ is low. Also, from Fig. 9, we can see that $\mathcal{P}_{\text{to}}$ decays as the Nakagami parameters m_0 and m become larger.

In Figs. 10 and 11, the transmission outage probabilities $\mathcal{P}_{\text{to}}$

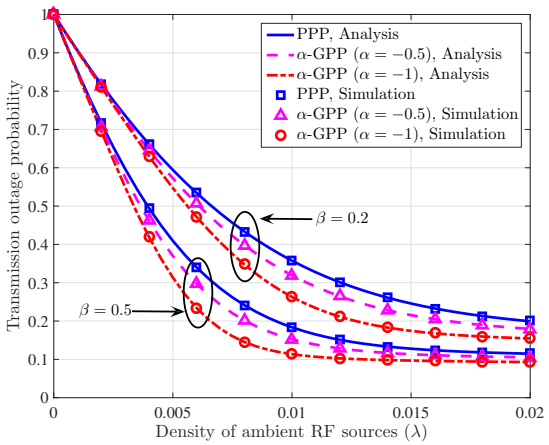

Fig. 8. Transmission outage probability $\mathcal{P}_{\rm to}$ as a function of λ ($d_0 = 3, C_{\rm th} = 0.002$ and $\xi = 1$)

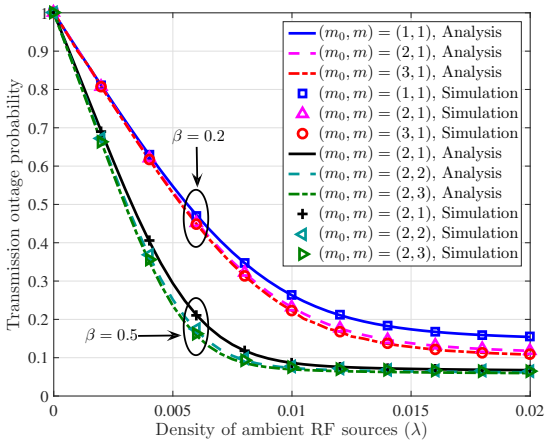

Fig. 9. Transmission outage probability $\mathcal{P}_{\rm to}$ as a function of λ when $m_0 \geq 1$ ($d_0 = 3, C_{\rm th} = 0.002$ and $\xi = 1$)

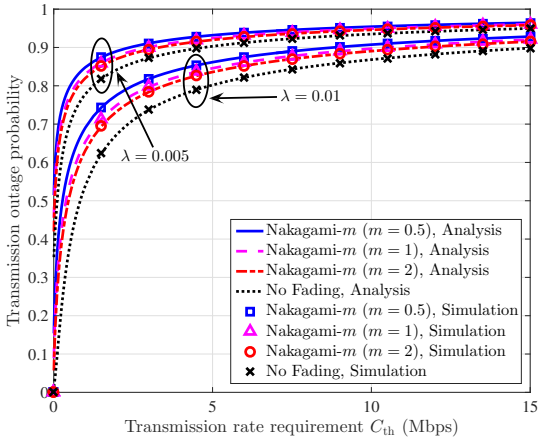

Fig. 10. Transmission outage probability $\mathcal{P}_{\rm to}$ as a function of $C_{\rm th}$ ($d_0 = 10$ and $\xi = 0$)

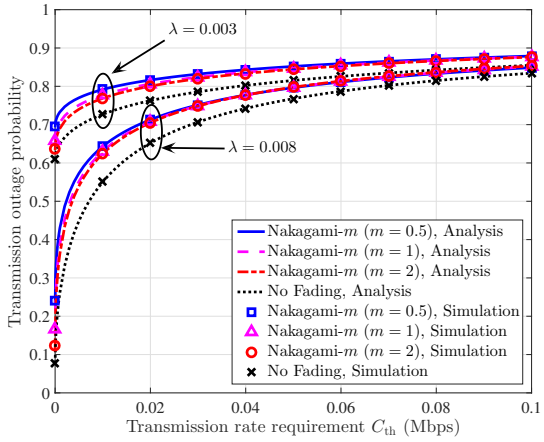

Fig. 11. Transmission outage probability $\mathcal{P}_{\rm to}$ as a function of $C_{\rm th}$ ($d_0 = 5$ and $\xi = 1$)

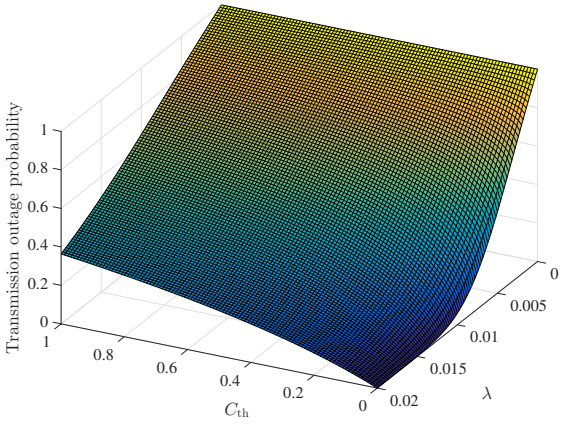

Fig. 12. Transmission outage probability $\mathcal{P}_{\rm to}$ as functions of λ and $C_{\rm th}$ ($d_0 = 20$ and $\xi = 0$)

are demonstrated as a function of $C_{\rm th}$ with various values of λ. It is shown that the analytical results are very accurate for different m and λ. The transmission outage probability grows almost logarithmically as the threshold $C_{\rm th}$ increases. Thus, $\mathcal{P}_{\rm to}$ is very sensitive to $C_{\rm th}$ when $C_{\rm th}$ is small, and $\mathcal{P}_{\rm to}$ varies slowly when $C_{\rm th}$ is high. Also, as observed in Figs. 7 to 9, a larger λ results in a lower outage probability. Moreover, we can see that a smaller m leads to a higher transmission outage probability, and the impact of m is more pronounced when λ is large.

Figs. 12 and 13 examine the influence of λ and $C_{\rm th}$ on the transmission outage probability $\mathcal{P}_{\rm to}$. For the out-of-band transmission ($\xi = 0$), as there is no interference at the data sink from the ambient RF sources, $\mathcal{P}_{\rm to}$ quickly decreases as λ grows in all $C_{\rm th}$ region. However, for the in-band transmission ($\xi = 1$), due to the existence of interference, $\mathcal{P}_{\rm to}$ is saturated except for networks with a small $C_{\rm th}$. In contrast to $\mathcal{P}_{\rm po}$ in Fig. 6, the transmission outage probability does not converge to 0 when the threshold value goes to 0, and it converges to a certain probability. This converged probability can be interpreted as the probability that the sensor node fails to

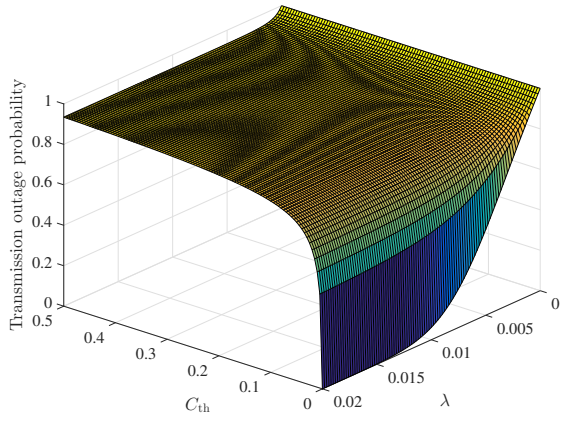

Fig. 13. Transmission outage probability $\mathcal{P}_{\rm to}$ as functions of λ and $C_{\rm th}$ ($d_0 = 5$ and $\xi = 1$)

harvest enough power to transmit data to the data sink, i.e., the power outage probability. In addition, for both transmission cases, we can observe that $\mathcal{P}_{\rm to}$ is more susceptible to λ (respectively $C_{\rm th}$) when $C_{\rm th}$ is small (respectively λ is large).

VI. Conclusion

In this paper, we have analyzed the performance of ambient RF energy harvesting sensor networks where the distribution of ambient RF sources is modeled as an α-GPP which reflects the repulsion among the sources and includes a PPP as a special case. We have first derived the Laplace transform of the α-GPP which is represented in terms of the Fredholm determinant. Since a conventional method to compute the Fredholm determinant may have a high computational cost, we have introduced a new closed-form expression for the Fredholm determinant. Then, based on the derived Laplace transform of the α-GPP, we have provided semi-closed-form expressions for the mean of the harvested energy, the exact power outage probability and the PDF of the harvested energy. Also, we have derived a computationally-efficient closed-form expression for an upper bound of the power outage probability. Additionally, by utilizing the obtained PDF, we have analyzed the exact transmission outage probability in the networks. By extensive numerical simulations, we have verified that our derived analytical results can predict accurately the performance of the networks.

Appendix A
Proof of Lemma 3

We set

$$\rho_n = \frac{2\,(\pi\lambda)^{n+1}}{n!}\int_0^R q(r)^2 \exp(-\pi\lambda r^2) r^{2n+1}\,dr,$$

and

$$\phi_n(\mathbf{x}) := \sqrt{\frac{\lambda}{\rho_n n!}} q(\|\mathbf{x}\|)\left(\sqrt{\pi\lambda}\mathbf{x}\right)^n \exp\left(-\frac{\pi\lambda}{2}\|\mathbf{x}\|^2\right),$$

for $\mathbf{x} \in \mathbb{R}^2$ and $n \geq 0$. Then, it is readily checked that

$$K_q(\mathbf{x},\mathbf{y}) = \sum_{n\geq 0} \rho_n \phi_n(\mathbf{x})\overline{\phi_n(\mathbf{y})}, \quad \mathbf{x},\mathbf{y}\in\mathbb{R}^2,$$

and $\{\phi_n\}$ is an orthonormal set, in the sense that $\int_{\mathbb{R}^2} |\phi_n(\mathbf{x})|^2\,d\mathbf{x} = 1$ for all $n \geq 0$ and $\int_{\mathbb{R}^2} \phi_n(\mathbf{x})\overline{\phi_m(\mathbf{x})}\,d\mathbf{x} = 0$ for $n \neq m$. For any $n \geq 0$, it follows that

$$\begin{aligned}\int_{\mathbb{R}^2} K_q(\mathbf{x},\mathbf{y})\phi_n(\mathbf{y})\,d\mathbf{y} &= \sum_{m\geq 0}\rho_m\phi_m(\mathbf{x})\int_{\mathbb{R}^2}\overline{\phi_m(\mathbf{y})}\phi_n(\mathbf{y})\,d\mathbf{y}\\ &= \rho_n\phi_n(\mathbf{x}),\end{aligned}$$

which means by definition that ρ_n is an eigenvalue of the integral operator defined in (6), and ϕ_n is the corresponding eigenvector. The result follows since in that case, it is known that

$$\mathrm{Det}(I + \alpha K_q) = \prod_{n\geq 0}(1+\alpha\rho_n). \qquad \blacksquare$$

Appendix B
Proof of Theorem 2

The MGF of a gamma random variable $X \sim \mathcal{G}(a,b)$ is equal to $M_X(t) = (1-bt)^{-a}$. Therefore, when $h_k \sim \mathcal{G}(m,\theta/m)$, from Lemma 2, the Laplace transform of the harvested energy $P_H = \beta P_A \sum_{k\in\Phi} h_k d_k^{-l}$ becomes

$$\begin{aligned}\mathcal{L}_{P_H}(s) =& \mathbb{E}\left[\exp\Big(-s\beta P_A\sum_{k\in\Phi} h_k d_k^{-l}\Big)\right]\\ =& \mathrm{Det}\left(I + \alpha A_s\right)^{-1/\alpha},\end{aligned} \tag{32}$$

where A_s is the kernel defined in (19). In addition, when h_k is a constant as $h_k = \theta$, Lemma 1 shows that the kernel of A_s is given by (20).

Given the Laplace transforms in (32), we identify the PDF of P_H by employing the inverse Laplace method [46] as

$$f_{P_H}(x) = \mathcal{L}^{-1}\left\{\mathcal{L}_{P_H}(s)\right\}(x). \tag{33}$$

Combining (32) and (33), we derive the result in (21). Also, by integrating the PDF, we obtain the CDF of P_H as

$$F_{P_H}(x) = \int_{-\infty}^{x}\mathcal{L}^{-1}\left\{\mathcal{L}_{P_H}(s)\right\}(t)dt = \mathcal{L}^{-1}\left\{\frac{1}{s}\mathcal{L}_{P_H}(s)\right\}(x).$$

From the definition of $\mathcal{P}_{\rm po}$ in (4), $\mathcal{P}_{\rm po}$ is equal to $F_{P_H}(P_{\rm th})$, which yields (17). This concludes the proof. $\blacksquare$

Appendix C
Proof of Theorem 3

Since $\{h_k\}$ and Φ are independent, we derive an upper bound of $\mathcal{P}_{\rm to}$ as

$$\begin{aligned}\mathcal{P}_{\rm to} &= \mathbb{P}\left(\sum_{k\in\Phi} h_k d_k^{-l} < \frac{P_{\rm th}}{\beta P_A}\right)\\ &\leq \mathbb{P}\left(\forall k\in\Phi, h_k d_k^{-l} < \frac{P_{\rm th}}{\beta P_A}\right)\\ &= \mathbb{E}\left[\mathbb{P}\left(\forall k\in\Phi, h_k d_k^{-l} < \frac{P_{\rm th}}{\beta P_A}|\Phi\right)\right]\\ &= \mathbb{E}\left[\prod_{k\in\Phi}\mathbb{P}\left(h_k < \frac{P_{\rm th} d_k^l}{\beta P_A}\right)\right].\end{aligned} \tag{34}$$

Note that the CDF of a gamma distributed random variable $X \sim \mathcal{G}(a,b)$ is $\mathbb{P}(X<x)=\frac{\gamma\left(a,\frac{x}{b}\right)}{\Gamma(a)}$. Thus, the above upper bound becomes

$$\begin{aligned}\mathcal{P}_{\rm to} &\le \mathbb{E}\left[\prod_{k\in\Phi}\frac{\gamma\left(m,\frac{mP_{\rm th}d_k^l}{\beta\theta P_A}\right)}{\Gamma(m)}\right]\\ &= \mathbb{E}\left[\exp\left(\sum_{k\in\Phi}\ln\left(\frac{\gamma\left(m,\frac{mP_{\rm th}d_k^l}{\beta\theta P_A}\right)}{\Gamma(m)}\right)\right)\right].\end{aligned}$$

From (11), we find that the above upper bound is equal to (22). ∎

Appendix D
Proof of Theorem 4

As $h_0 \sim \mathcal{E}(1/\theta_0)$, the CDF of h_0 is $\mathbb{P}(h_0<x)=1-\exp(-x/\theta_0)$. Thus, we compute $\tilde{\mathcal{P}}_{\rm to}$ in (24) as

$$\begin{aligned}\tilde{\mathcal{P}}_{\rm to} =&\mathbb{P}\left(\frac{P_T h_0 d_0^{-l}}{\xi Q+\sigma^2}<\eta, P_H\ge P_{\rm th}\right)\\ =&\mathbb{E}\left[\mathbb{P}\left(\frac{P_T h_0 d_0^{-l}}{\xi Q+\sigma^2}<\eta\middle|P_H\right)\mathbb{1}_{\{P_H\ge P_{\rm th}\}}\right]\\ =&\mathbb{E}\left[\mathbb{P}\left(h_0<\frac{\eta d_0^l\left(\xi Q+\sigma^2\right)}{P_T}\middle|P_H\right)\mathbb{1}_{\{P_H\ge P_{\rm th}\}}\right]\\ =&\mathbb{E}\left[\left(1-\exp\left(-\frac{\eta d_0^l\left(\xi Q+\sigma^2\right)}{\theta_0 P_T}\right)\right)\mathbb{1}_{\{P_H\ge P_{\rm th}\}}\right]\\ =&\mathbb{P}\left(P_H\ge P_{\rm th}\right)\\ &-\mathbb{E}\left[\exp\left(-\frac{\eta d_0^l\left(\xi Q+\sigma^2\right)}{\theta_0 P_T}\right)\mathbb{1}_{\{P_H\ge P_{\rm th}\}}\right], \quad (35)\end{aligned}$$

where $\mathbb{1}_{\{\cdot\}}$ denotes the indicator function. Combining (23) and (35), we have

$$\begin{aligned}&\mathcal{P}_{\rm to}\\ =&1-\mathbb{E}\left[\exp\left(-\frac{\eta d_0^l\left(\xi Q+\sigma^2\right)}{\theta_0 P_T}\right)\mathbb{1}_{\{P_H\ge P_{\rm th}\}}\right] \quad (36)\\ =&1-\mathbb{E}\Bigg[\exp\left(-\frac{\eta d_0^l\sigma^2}{\theta_0 P_T}\right)\\ &\times\mathbb{E}\left[\exp\left(-\frac{\eta d_0^l\xi P_A}{\theta_0 P_T}\sum_{k\in\tilde{\Phi}}\tilde{h}_k\tilde{d}_k^{-l}\right)\mid P_H\right]\mathbb{1}_{\{P_H\ge P_{\rm th}\}}\Bigg]\\ \overset{\rm (e)}{=}&1-\mathbb{E}\left[\exp\left(-\frac{\eta d_0^l\sigma^2}{\theta_0 P_T}\right)\mathrm{Det}\left(I+\alpha C_{P_H}\right)^{-1/\alpha}\mathbb{1}_{\{P_H\ge P_{\rm th}\}}\right] \quad (37)\\ =&1-\int_{P_{\rm th}}^{\infty}\exp\left(-\frac{\eta d_0^l\sigma^2}{\theta_0\left(x-P_{\rm th}\right)}\right)\mathrm{Det}\left(I+\alpha C_x\right)^{-1/\alpha}f_{P_H}(x)\,dx,\end{aligned}$$

where C_x is the kernel defined in (26). Here, (e) comes from Lemma 2 and the stationarity of the α-GPP $\tilde{\Phi}$ (cf. Section III-B). ∎

Appendix E
Computation of $\mathcal{P}_{\rm to}$ when Φ and $\tilde{\Phi}$ are the same point processes

Now, we briefly investigate the case where the locations of the ambient RF sources in two phases (Φ and $\tilde{\Phi}$) are the same. In this case, as P_H in (1) and Q in (24) are correlated, deriving an analytical representation of $\mathcal{P}_{\rm to}$ is much more challenging. First, from (36), we have

$$\mathcal{P}_{\rm to}=1-\mathbb{E}\left[\Omega(P_H,Q)\right],$$

where $\Omega(x,y)\triangleq\exp\left(-\frac{\eta d_0^l\left(\xi y+\sigma^2\right)}{\theta_0\left(x-P_{\rm th}\right)}\right)\mathbb{1}_{\{x\ge P_{\rm th}\}}$. Note that, for $s,t\ge 0$, the bi-dimensional Laplace transform of (P_H,Q) can be derived as

$$\begin{aligned}&\mathbb{E}\left[\exp\left(-sP_H-tQ\right)\right]\\ &=\mathbb{E}\left[\exp\left(-\sum_{k\in\Phi}\left(s\beta P_A h_k d_k^{-l}+tP_A\tilde{h}_k\tilde{d}_k^{-l}\right)\right)\right]\\ &=\mathbb{E}\left[\prod_{k\in\Phi}\mathbb{E}\left[\exp\left(-s\beta P_A h_k d_k^{-l}\right)\right]\mathbb{E}\left[\exp\left(-tP_A\tilde{h}_k\tilde{d}_k^{-l}\right)\right]\right]\\ &=\mathbb{E}\Bigg[\prod_{k\in\Phi}\left(1+\frac{s\beta\theta P_A}{m(||\mathbf{x}_k||+\epsilon)^l}\right)^{-m}\\ &\qquad\times\left(1+\frac{t\theta P_A}{m(||\mathbf{x}_k-\mathbf{x}_{ds}||+\epsilon)^l}\right)^{-m}\Bigg]\\ &=\mathrm{Det}\left(I+\alpha G_{s,t}\right)^{-\frac{1}{\alpha}},\end{aligned}$$

where $G_{s,t}$ is the kernel defined as

$$\begin{aligned}&G_{s,t}(\mathbf{x},\mathbf{y})\\ &=\sqrt{1-\left(1+\frac{s\beta\theta P_A}{m(||\mathbf{x}||+\epsilon)^l}\right)^{-m}\left(1+\frac{t\theta P_A}{m(||\mathbf{x}-\mathbf{x}_{ds}||+\epsilon)^l}\right)^{-m}}\\ &\times K(\mathbf{x},\mathbf{y})\\ &\times\sqrt{1-\left(1+\frac{s\beta\theta P_A}{m(||\mathbf{y}||+\epsilon)^l}\right)^{-m}\left(1+\frac{t\theta P_A}{m(||\mathbf{y}-\mathbf{x}_{ds}||+\epsilon)^l}\right)^{-m}},\end{aligned}$$

for $\mathbf{x},\mathbf{y}\in\mathbb{R}^2$. Then, the joint PDF of (P_H,Q) can be obtained by inverting the bi-dimensional Laplace transform according to

$$\begin{aligned}f_{(P_H,Q)}(x,y)&=\mathcal{L}^{-1}_{(P_H,Q)}(x,y)\\ &=\left(\frac{1}{2\pi i}\right)^2\int_{c-i\infty}^{c+i\infty}\int_{c'-i\infty}^{c'+i\infty}\exp\left(sx+ty\right)\\ &\qquad\times\mathrm{Det}\left(I+\alpha G_{s,t}\right)^{-\frac{1}{\alpha}}\,\mathrm{d}s\,\mathrm{d}t,\end{aligned}$$

$x,y\in[0,\infty)$, see [47]. Finally, we have

$$\begin{aligned}\mathcal{P}_{\rm to}&=1-\int_0^\infty\int_0^\infty\Omega(x,y)f_{(P_H,Q)}(x,y)\,\mathrm{d}x\,\mathrm{d}y\\ &=1-\int_0^\infty\int_{P_{\rm th}}^\infty\exp\left(-\frac{\eta d_0^l\left(\xi y+\sigma^2\right)}{\theta_0(x-P_{\rm th})}\right)\\ &\qquad\times f_{(P_H,Q)}(x,y)\,\mathrm{d}x\,\mathrm{d}y.\end{aligned}$$

Note that the above expression is too complicated, i.e., it contains the double integral operation and the integrand consists of the bi-dimensional inverse Lapalce transform of the Fredholm determinant. Therefore, identifiying an efficient way to compute $\mathcal{P}_{\rm to}$ for networks where Φ and $\tilde{\Phi}$ are the same is a challenging issue which is left for future work. ■

Appendix F
Proof of Theorem 5

Note that the CDF of h_0 is given by $\mathbb{P}\left(h_0 < x\right) = 1 - \sum_{i=0}^{m_0-1} \frac{1}{i!}\left(\frac{m_0 x}{\theta_0}\right)^i \exp(-\frac{m_0 x}{\theta_0})$. Then, in a similar way to (37), the transmission outage probability is expressed as

$$\mathcal{P}_{\rm to} = 1 - \sum_{i=0}^{m_0-1} \frac{1}{i!}\left(\frac{m_0}{\theta_0}\right)^i \mathbb{E}\left[\left(\frac{\eta d_0^l}{P_T}\right)^i \Psi_{Q,i} \mathbb{1}_{\{P_H \geq P_{\rm th}\}}\right], \tag{38}$$

where

$$\Psi_{Q,i} = \mathbb{E}\left[\left(\xi Q + \sigma^2\right)^i \exp\left(-\frac{m_0 \eta d_0^l \left(\xi Q + \sigma^2\right)}{\theta_0 P_T}\right)\right]. \tag{39}$$

Denoting by $\mathcal{L}_X(s)$ the Laplace transform of a random variable X, we have $\mathbb{E}\left[X^i \exp\left(-sX\right)\right] = (-1)^i \mathcal{L}_X^{(i)}(s)$ where $\mathcal{L}_X^{(i)}(s)$ stands for the i-th derivative of $\mathcal{L}_X(s)$. Hence, by Lemma 2, $\Psi_{Q,i}$ in (39) becomes

$$\begin{aligned}\Psi_{Q,i} &= (-1)^i \frac{\partial^i \{\mathbb{E}[\exp(-\mu\xi Q)]\exp(-\mu\sigma^2)\}}{\partial \mu^i} \\ &\overset{\rm (f)}{=} (-1)^i \frac{\partial^i \{\mathrm{Det}\left(I + \alpha D_{\mu\xi P_A}\right)^{-1/\alpha} \exp(-\mu\sigma^2)\}}{\partial \mu^i},\end{aligned} \tag{40}$$

where $\mu \triangleq \frac{m_0 \eta d_0^l}{\theta_0 P_T}$ and D_s is the kernel defined in (28). Here, (f) follows from (11) and the fact that the α-GPP $\tilde{\Phi}$ is stationary.

Then, combining (38) and (40), we have

$$\begin{aligned}\mathcal{P}_{\rm to} = 1 - \sum_{i=0}^{m_0-1} \frac{1}{i!}\left(-\frac{m_0}{\theta_0}\right)^i \int_{P_{\rm th}}^{\infty} \left(\frac{\eta d_0^l}{x - P_{\rm th}}\right)^i \\ \times \frac{\partial^i \{\mathrm{Det}\left(I + \alpha D_{\mu_x \xi P_A}\right)^{-1/\alpha} \exp(-\mu_x \sigma^2)\}}{\partial \mu_x^i} f_{P_H}(x)\, dx,\end{aligned} \tag{41}$$

where $\mu_x \triangleq \frac{m_0 \eta d_0^l}{\theta_0 (x - P_{\rm th})}$. Unfortunately, it is difficult to identify a closed-form expression for the i-th derivative of the Fredholm determinant. Therefore, as a method to evaluate the i-th derivative of the Fredholm determinant, we employ the i-th order central difference operator which computes the i-th derivative of a function $\varphi(x)$ as [48]

$$\frac{\partial^i \{\varphi(x)\}}{\partial x^i} = \lim_{\tau \to 0} \frac{1}{\tau^i} \sum_{j=0}^{i} (-1)^{i-j} \binom{i}{j} \varphi\left(x + \tau\left(j - \frac{i}{2}\right)\right). \tag{42}$$

By substituting (42) into (41), we obtain (27). ■

Appendix G
Proof of Theorem 6

We first focus on the in-band transmission case ($\xi = 1$). When the fading channels are constant, Q is equal to $Q = P_A \theta \sum_{k \in \tilde{\Phi}} \tilde{d}_k^{-l}$ and $\tilde{\mathcal{P}}_{\rm to}$ in (24) becomes

$$\begin{aligned}\tilde{\mathcal{P}}_{\rm to} &= \mathbb{P}\left(\frac{P_T \theta_0 d_0^{-l}}{Q + \sigma^2} < \eta, P_H \geq P_{\rm th}\right) \\ &= \mathbb{P}\left(Q > \frac{\theta_0 P_T}{\eta d_0^l} - \sigma^2, P_H \geq P_{\rm th}\right) \\ &= \mathbb{E}\left[\mathbb{P}\left(Q > \frac{\theta_0 P_T}{\eta d_0^l} - \sigma^2 \,\middle|\, P_H\right) \mathbb{1}_{\{P_H \geq P_{\rm th}\}}\right] \\ &= \mathbb{E}\left[\left(1 - F_Q\left(\frac{\theta_0 P_T}{\eta d_0^l} - \sigma^2\right)\right) \mathbb{1}_{\{P_H \geq P_{\rm th}\}}\right] \\ &= \mathbb{P}\left(P_H \geq P_{\rm th}\right) \\ &\quad - \int_{c_2}^{\infty} F_Q\left(\frac{\theta_0 \left(x - P_{\rm th}\right)}{\eta d_0^l} - \sigma^2\right) f_{P_H}(x)\, dx,\end{aligned} \tag{43}$$

where $F_Q(x)$ is the CDF of Q which is calculated as

$$F_Q(x) = \mathcal{L}^{-1}\left\{\frac{1}{s}\mathcal{L}_Q(s)\right\}(x).$$

Here, $\mathcal{L}_Q(s)$ stands for the Laplace transform of Q. From the result in Lemma 1 and the stationarity of the α-GPP $\tilde{\Phi}$, $\mathcal{L}_Q(s)$ can be written as

$$\begin{aligned}\mathcal{L}_Q(s) &= \mathbb{E}\left[\exp\Big(-s\theta P_A \sum_{k \in \tilde{\Phi}} \tilde{d}_k^{-l}\Big)\right] \\ &= \mathrm{Det}\left(I + \alpha E_s\right)^{-1/\alpha},\end{aligned}$$

where E_s is the kernel defined in (30). Combining the results in (23) and (43), we obtain (29).

When $\xi = 0$, $\tilde{\mathcal{P}}_{\rm to}$ in (24) becomes

$$\begin{aligned}\tilde{\mathcal{P}}_{\rm to} &= \mathbb{P}\left(P_T < \frac{\eta \sigma^2 d_0^l}{\theta_0}, P_H \geq P_{\rm th}\right) \\ &= \mathbb{P}\left(P_H < P_{\rm th} + \frac{\eta \sigma^2 d_0^l}{\theta_0}, P_H \geq P_{\rm th}\right) \\ &= \mathbb{P}\left(P_{\rm th} \leq P_H < P_{\rm th} + \frac{\eta \sigma^2 d_0^l}{\theta_0}\right) \\ &= F_{P_H}\left(P_{\rm th} + \frac{\eta \sigma^2 d_0^l}{\theta_0}\right) - \mathbb{P}\left(P_H \leq P_{\rm th}\right).\end{aligned} \tag{44}$$

Plugging (44) into (23), we obtain (31), which concludes the proof. ■

References

[1] X. Lu, P. Wang, D. Niyato, D. I. Kim, and Z. Han, "Wireless Networks With RF Energy Harvesting: A Contemporary Survey," *IEEE Commun. Surv. Tut.*, vol. 17, pp. 757–789, Second Quarter 2015.

[2] M. M. Tentzeris and Y. Kawahara, "Design Optimization and Implementation for RF Energy Harvesting Circuits," *IEEE J. Emerg. Sel. Topics Circuits Syst.*, vol. 2, pp. 24–33, Mar. 2012.

[3] H. Nishimoto, Y. Kawahara, and T. Asami, "Prototype Implementation of Ambient RF Energy Harvesting Wireless Sensor Networks," in *Proc. IEEE Sensor*, Kona, HI, USA, pp. 1282-1287, Nov. 2010.

[4] X. Zhang, H. Jiang, L. Zhang, C. Zhang, Z. Wang, and X. Chen, "An Energy-Efficient ASIC for Wireless Body Sensor Networks in Medical Applications," *IEEE Trans. Biomed. Circuits Syst.*, vol. 4, pp. 11–18, Feb. 2010.

[5] X. Lu, D. Niyato, P. Wang, D. I. Kim, and Z. Han, "Wireless Charger Networking for Mobile Devices: Fundamentals, Standards, and Applications," *IEEE Wireless Commun.*, vol. 22, pp. 126–135, Apr. 2015.

[6] A. N. Parks, A. P. Sample, Y. Zhao, and J. R. Smith, "A Wireless Sensing Platform Utilizing Ambient RF Energy," in *Proc. BioWireleSS*, pp. 154–156, 2013.

[7] R. Zhang and C. K. Ho, "MIMO Broadcasting for Simultaneous Wireless Information and Power Transfer," *IEEE Trans. Wireless Commun.*, vol. 12, pp. 1989–2001, May 2013.

[8] S. Timotheou, I. Krikidis, G. Zheng, and B. Ottersten, "Beamforming for MISO Interference Channels with QoS and RF Energy Transfer," *IEEE Trans. Wireless Commun.*, vol. 13, pp. 2646–2658, May 2014.

[9] H. Lee, S.-R. Lee, K.-J. Lee, H.-B. Kong, and I. Lee, "Optimal Beamforming Designs for Wireless Information and Power Transfer in MISO Interference Channels," *IEEE Trans. Wireless Commun.*, vol. 9, pp. 4810–4821, Sep. 2015.

[10] J. Park and B. Clerckx, "Joint Wireless Information and Energy Transfer in a K-User MIMO Interference Channel," *IEEE Trans. Wireless Commun.*, vol. 13, pp. 5781–5796, Oct. 2014.

[11] C. S. X. L. Q. Sun, G. Zhu and Z. Zhong, "Joint Beamforming Design and Time Allocation for Wireless Powered Communication Networks," *IEEE Commun. Lett.*, vol. 18, pp. 1783–1786, Oct. 2014.

[12] U. Olgun, C.-C. Chen, and J. L. Volakis, "Design of an Efficient Ambient WiFi Energy Harvesting System," *IET Microw. Antennas Propag.*, vol. 6, pp. 1200–1206, Aug. 2012.

[13] M. Pinuela, P. D. Mitcheson, and S. Lucyszyn, "Ambient RF Energy Harvesting in Urban and Semi-urban Environments," *IEEE Trans. Microw. Theory Techn.*, vol. 61, pp. 2715–2726, Jul. 2013.

[14] P. Nintanavongsa, M. Y. Naderi, and K. R. Chowdhury, "A Dual-Band Wireless Energy Transfer Protocol for Heterogeneous Sensor Networks Powered by RF Energy Harvesting," in *Proc. IEEE ICSEC*, Nakorn Pathom, Thailand, pp. 387-392, Sep. 2013.

[15] B. G. Karthik, S. Shivaraman, and V. Aditya, "Wi-Pie: Energy Harvesting in Mobile Electronic Devices," in *Proc. IEEE GHTC*, Seattle, WA, USA, pp. 398-401, Nov. 2011.

[16] K. Huang and V. K. N. Lau, "Enabling Wireless Power Transfer in Cellular Networks: Architecture, Modeling and Deployment," *IEEE Trans. Wireless Commun.*, vol. 13, pp. 902–912, Feb. 2014.

[17] A. H. Sakr and E. Hossain, "Analysis of K-Tier Uplink Cellular Networks With Ambient RF Energy Harvesting," *IEEE J. Sel. Areas Commun.*, vol. 33, pp. 2226–2238, Oct. 2015.

[18] I. Krikidis, "Simultaneous Information and Energy Transfer in Large-Scale Networks With/Without Relaying," *IEEE Trans. Commun.*, vol. 62, pp. 900–912, Mar. 2014.

[19] I. Krikidis, "Relay Selection in Wireless Powered Cooperative Networks With Energy Storage," *IEEE J. Sel. Areas Commun.*, vol. 33, pp. 2596–2610, Dec. 2015.

[20] Z. Ding, I. Krikidis, B. Sharif, and H. V. Poor, "Wireless Information and Power Transfer in Cooperative Networks With Spatially Random Relays," *IEEE Trans. Wireless Commun.*, vol. 13, pp. 4440–4453, Aug. 2014.

[21] P.-V. Mekikis, A. S. Lalos, A. Antonopoulos, L. Alonso, and C. Verikoukis, "Wireless Energy Harvesting in Two-Way Network Coded Cooperative Communications: A Stochastic Approach for Large Scale Networks," *IEEE Commun. Lett.*, vol. 18, pp. 1011–1014, Jun. 2014.

[22] A. H. Sakr and E. Hossain, "Cognitive and Energy Harvesting-Based D2D Communication in Cellular Networks: Stochastic Geometry Modeling and Analysis," *IEEE Trans. Commun.*, vol. 63, pp. 1867–1880, May 2015.

[23] S. Lee, R. Zhang, and K. Huang, "Opportunistic Wireless Energy Harvesting in Cognitive Radio Networks," *IEEE Trans. Wireless Commun.*, vol. 12, pp. 4788–4799, Sep. 2013.

[24] J. Guo, S. Durrani, X. Zhou, and H. Yanikomeroglu, "Outage Probability of Ad Hoc Networks With Wireless Information and Power Transfer," *IEEE Wireless Commun. Lett.*, vol. 4, pp. 409–412, Aug. 2015.

[25] T.-Y. Lin, H. Santoso, and K.-R. Wu, "Global Sensor Deployment and Local Coverage-Aware Recovery Schemes for Smart Environments," *IEEE Trans. Mobile Comput.*, vol. 14, pp. 1382–1396, Jul. 2015.

[26] S.-R. Cho and W. Choi, "Energy-Efficient Repulsive Cell Activation for Heterogeneous Cellular Networks," *IEEE J. Sel. Areas Commun.*, vol. 31, pp. 870–882, May 2013.

[27] N. Vastardis and K. Yang, "An Enhanced Community-Based Mobility Model for Distributed Mobile Social Networks," *J. Ambient Intell. and Humanized Comput.*, vol. 5, pp. 65–75, Feb. 2014.

[28] M. Haenggi, *Stochastic Geometry for Wireless Networks*. Cambridge, U.K.: Cambridge Univ. Press, 2012.

[29] A. Guo and M. Haenggi, "Spatial Stochastic Models and Metrics for the Structure of Base Stations in Cellular Networks," *IEEE Trans. Wireless Commun.*, vol. 12, pp. 5800–5812, Nov. 2013.

[30] Y. Li, F. Baccelli, H. S. Dhillon, and J. G. Andrews, "Statistical Modeling and Probabilistic Analysis of Cellular Networks With Determinantal Point Processes," *IEEE Trans. Commun.*, vol. 63, pp. 3405–3422, Sep. 2015.

[31] N. Deng, W. Zhou, and M. Haenggi, "The Ginibre Point Process as a Model for Wireless Networks With Repulsion," *IEEE Trans. Wireless Commun.*, vol. 14, pp. 107–121, Jan. 2015.

[32] I. Nakata and N. Miyoshi, "Spatial Stochastic Models for Analysis of Heterogeneous Cellular Networks with Repulsively Deployed Base Stations," *Performance Evaluation*, vol. 78, pp. 7–17, Aug. 2014.

[33] J. S. Gomez, A. Vasseur, A. Vergne, P. Martins, L. Decreusefond, and W. Chen, "A Case Study on Regularity in Cellular Network Deployment," *IEEE Wireless Commun. Lett.*, vol. 4, pp. 421–424, Aug. 2015.

[34] I. Flint, X. Lu, N. Privault, D. Niyato, and P. Wang, "Performance Analysis of Ambient RF Energy Harvesting With Repulsive Point Process Modeling," *IEEE Trans. Wireless Commun.*, vol. 14, pp. 5402–5416, Oct. 2015.

[35] A. Goldman, "The Palm Measure and the Voronoi Tessellation for the Ginibre Process," *Ann. Appl. Probab.*, vol. 20, pp. 90–128, 2010.

[36] T. Shirai and Y. Takahashi, "Random Point Fields Associated With Certain Fredholm Determinants I: Fermion, Poisson and Boson Point Processes," *J. Functional Anal.*, vol. 205, pp. 414–463, Apr. 2003.

[37] H. Inaltekin, S. B. Wicker, M. Chiang, and H. V. Poor, "On Unbounded Path-loss Models: Effects of Singularity on Wireless Network Performance," *IEEE J. Sel. Areas Commun.*, vol. 27, pp. 1078–1092, Sep. 2009.

[38] G. Miao, N. Himayat, Y. G. Li, and A. Swami, "Cross-layer Optimization for Energy-Efficient Wireless Communications: A Survey," *Wireless Commun. Mobile Comput.*, vol. 9, pp. 529–542, Apr. 2009.

[39] O. Kallenberg, *Random Measures*. Fourth Edition, Berlin, Germany: Akademie-Verlag, 1986.

[40] D. J. Daley and D. Vere-Jones, *An Introduction to the Theory of Point Processes: Volume I: Elementary Theory and Methods*. Second Edition, New York: Springer, 2003.

[41] L. Decreusefond, I. Flint, and A. Vergne, "Efficient Simulation of the Ginibre Point Process," *Adv. Appl. Probab.*, vol. 52, pp. 1–21, Oct. 2015.

[42] F. Bornemann, "On the Numerical Evaluation of Fredholm Determinants," 2008. Available: http://arxiv.org/abs/0804.2543.

[43] S. N. Chiu, D. Stoyan, W. S. Kendall, and J. Mecke, *Stochastic Geometry and Its Applications*. Third Edition, Wiley, 2013.

[44] K. J. Hollenbeck, *invlap.m: A Matlab Function for Numerical Inversion of Laplace Transforms by the de Hoog Algorithm*. http://www.isva.dtu.dk/staff/karl/invlap.htm, 1998.

[45] L. Liu, R. Zhang, and K. Chua, "Wireless Information and Power Transfer: A Dynamic Power Splitting Approach," *IEEE Trans. Commun.*, vol. 61, pp. 3990–4001, Sep. 2013.

[46] A. M. Cohen, *Numerical Methods for Laplace Transform Inversion*. Springer, 2007.

[47] A. Aghili and B. P. Moghaddam, "Certain Theorems on Two Dimensional Laplace Transform and Non-Homogeneous Parabolic Partial Differential Equations," *Surveys in Math. and its Applicat.*, vol. 6, pp. 165–174, 2011.

[48] T. Ström and J. N. Lyness, "On Numerical Differentiation," *BIT Numer. Math.*, vol. 15, pp. 1572–9125, Sep. 1975.